The dynamics of a swirling flow in a pipe and transition to axisymmetric vortex breakdown

By S. WANG AND Z. RUSAK

Department of Mechanical Engineering, Aeronautical Engineering and Mechanics,
Rensselaer Polytechnic Institute, Troy, NY 12180-3590, USA

This paper provides a new study of the axisymmetric vortex breakdown phenomenon. Our approach is based on a thorough investigation of the axisymmetric unsteady Euler equations which describe the dynamics of a swirling flow in a finite-length constant-area pipe. We study the stability characteristics as well as the time-asymptotic behaviour of the flow as it relates to the steady-state solutions. The results are established through a rigorous mathematical analysis and provide a solid theoretical understanding of the dynamics of an axisymmetric swirling flow. The stability and steady-state analyses suggest a consistent explanation of the mechanism leading to the axisymmetric vortex breakdown phenomenon in high-Reynolds-number swirling flows in a pipe. It is an evolution from an initial columnar swirling flow to another relatively stable equilibrium state which represents a flow around a separation zone. This evolution is the result of the loss of stability of the base columnar state when the swirl ratio of the incoming flow is near or above the critical level.

1. Introduction and mathematical model

1.1. *Introduction*

The term 'vortex breakdown' commonly refers to the abrupt and drastic change of structure which may occur under certain conditions in high-Reynolds-number swirling flows. This phenomenon is characterized by a sudden axial deceleration, that occurs above a certain level of swirl, leading to the formation of a free stagnation point which is followed by a separation region with turbulence behind it. Depending on the level of swirl (at a given Reynolds number) the breakdown may adopt a range of shapes, from asymmetric spiral waves to a nearly axisymmetric separation zone.

The scientific interest in explaining this strongly nonlinear phenomenon has led to many experimental, numerical and theoretical studies, and several review papers on this subject have been presented, including the reports by Hall (1972), Leibovich (1978, 1984), Escudier (1988) and Sarpkaya (1995). Although there has been extensive research, the fundamental nature of these phenomena still remains largely experimentally and theoretically unexplained.

The continued research toward understanding vortex breakdown has mainly been motivated by the field of aeronautics, mostly to reduce its harmful effects on slender aircraft configurations flying at high angles of attack (see Peckham & Atkinson 1957 and Lambourne & Bryer 1962). For a confined swirling flow through a pipe or in a closed container, vortex breakdown may have potential technological applications

min $\{w(x,0)\}$

Inviscid flow solutions:

Columnar flow	——————
Benjamin (1962)	●
Leibovich & Kribus (1990)	-----------
Keller *et al.* (1985)	■
Buntine & Saffman (1995)	———

Viscous flow solutions:

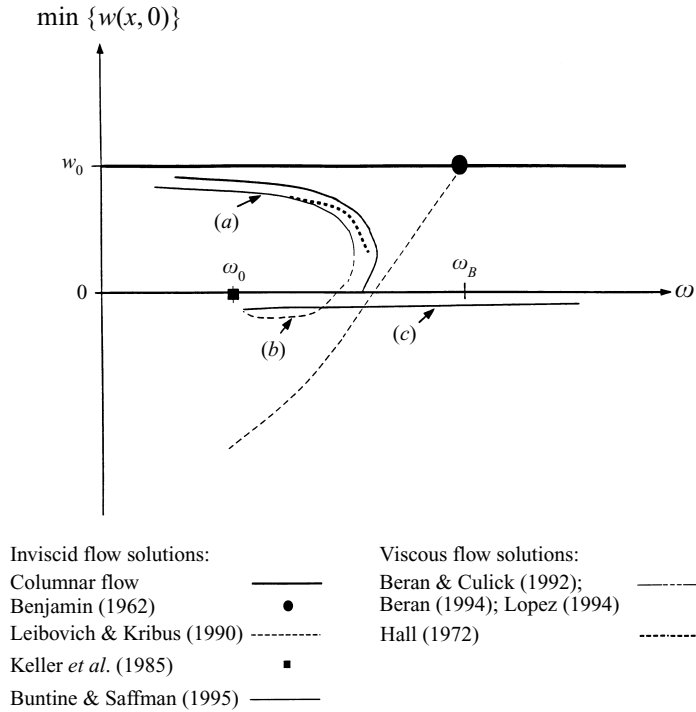|	
Beran & Culick (1992);	—–———
Beran (1994); Lopez (1994)	
Hall (1972)	----------

FIGURE 1. The bifurcation diagram: summary of previous theoretical studies.

such as flame stabilization in combustion chambers (see Escudier 1988). Vortex breakdown may also occur in hydrocyclon separators as well as in swirling jets behind nozzles, and is also common to the motion of atmospheric vortices such as tornados. Therefore, the ability to understand the complicated structures that develop as a consequence of vortex breakdown and to predict the flow conditions that lead to these phenomena would be essential for the future utilization of swirling flows in the design of advanced aerodynamic and hydromechanical devices where swirl has a dominant influence.

In this paper we concentrate on the axisymmetric breakdown phenomenon in a swirling flow in a constant-area pipe. A summary of previous theoretical analyses of this phenomenon is presented in the bifurcation diagram in figure 1. In this figure the vertical axis is the minimum of the axial velocity component, w, along the vortex centreline, the x-axis, that may be found in various steady-state solutions. The horizontal axis is the swirl level ω of the incoming flow to the pipe. It should be emphasized that when $\min(w(x,0)) \leqslant 0$ a stagnation point appears, followed by a separation zone.

In the case of an inviscid incompressible flow, we consider a branch of steady-state solutions describing a columnar axisymmetric swirling base flow throughout the pipe for any swirl level, ω, where the axial, radial and circumferential velocity components are given by $w = w_0(r)$, $u = 0$ and $v = \omega v_0(r)$, respectively. Here, r is the radial distance from the vortex centreline. For this branch of solutions, $\min(w(x,0)) = w_0(0)$ for every ω. Along this branch Squire (1960) and Benjamin (1962) identified a certain critical level of swirl, ω_B, where an infinitely long infinitesimal axisymmetric standing wave may appear (see figure 1). The critical-state theory of Benjamin (1962) relates the dynamical characteristics of a swirling columnar flow to its ability to sustain standing

axisymmetric small-disturbance waves. Supercritical vortex flows have low swirl ratios and are unable to support such waves, while subcritical flows having high swirl ratios can. Benjamin (1962) also used a variational principle for the flow equations and described the axisymmetric breakdown in a rather simple model, as a transition from an upstream supercritical columnar vortex flow to a downstream subcritical columnar flow, in analogy to the hydraulic jump in shallow water. Benjamin's theory predicts a change in the total head between these two columnar states which represents a change in mechanical energy.

Randall & Leibovich (1973) showed that the critical state is a singular state of the inviscid steady equations. Using a weakly nonlinear analysis they found a branch of steady-state axisymmetric solutions of the Euler equations which bifurcate from the columnar branch when $\omega < \omega_B$. These solutions describe a standing solitary wave that develops in a base swirling flow in an infinitely long straight pipe. Leibovich & Kribus (1990) showed, using numerical continuation methods, that this standing wave becomes larger and a closed separation zone may appear as the swirl is decreased from the critical level ω_B to zero. Since the flow in the separation zone is not connected by streamlines with the upstream flow, Leibovich & Kribus (1990) used the analytical continuation model to describe the flow inside the separation zone. For this branch of solutions, reversed flow develops in the separation zone and $\min(w(x,0))$ becomes negative as ω is reduced from ω_B to zero (see figure 1).

In another inviscid steady-state approach, Escudier & Keller (1983) and Keller, Egli & Exley (1985) described the axisymmetric vortex breakdown in an infinitely long straight pipe as an open stagnation zone of free boundaries that appears in the base vortex flow. Their solution describes a transition from a base upstream columnar state to another, downstream, columnar state that has the same 'flow force' (resulting from the conservation of axial momentum along the pipe); both states are solutions of the same columnar problem. However, a careful understanding of this solution shows that when the vortical core radius of the base (upstream) state is fixed, the solution is limited only to a specific value of the swirl, defined later in this paper as ω_0, where $\omega_0 < \omega_B$. For this special solution $\min(w(x,0)) = 0$ (see figure 1).

The effect of a changing the cross-sectional area of a tube on a stream of rotating fluid was studied in the work of Batchelor (1967). To the best of our knowledge, Batchelor (1967) is the first to notice that the solution families for inviscid swirling flows in a diverging pipe have a fold as swirl is increased. Batchelor's work has motivated a recent theoretical study by Buntine & Saffman (1995) who examined the development of inviscid steady swirling flows in a finite-length diverging pipe. They investigated the dependence of solutions on inlet and outlet boundary conditions and flow geometry. Their numerical computations result in an interesting bifurcation diagram when a parallel flow condition was imposed along the pipe outlet (see figure 1). There exists a limit point of swirl where the branch of solutions folds. Buntine & Saffman (1995) claimed that when a stagnation point appears along the pipe outlet non-regular solutions that should describe a separation zone must develop, and the flow inside the separation zone cannot be determined by the inlet conditions. They also raised the need to study the stability of the axisymmetric and inviscid flows in the vicinity of the limit point to clarify the influence of upstream conditions.

Hall (1967, 1972) used the quasi-cylindrical approximation to the steady and axisymmetric Navier–Stokes equations to describe a swirling flow with small streamwise gradients, from which he derived a parabolic equation that can be integrated along the pipe axis. He found that the flow along the pipe axis decelerates as the swirl increases (see figure 1) and there is a certain level of swirl above which no solution

of the parabolic equation can be found. This indicates that the assumption of small streamwise gradients is no longer valid, and vortex breakdown should be inferred, in analogy to the separation of a boundary layer.

Recent numerical computations by Beran & Culick (1992) have revealed a complicated bifurcation diagram of solutions of the steady and axisymmetric Navier–Stokes equations (see figure 1). They found that there exist two limit points of swirl when the Reynolds number is large enough. These limit points connect three branches of steady-state solutions of different types. Along the branch of solutions (*a*) the incoming swirl increases up to the first limit point and they describe a near columnar flow throughout the pipe. The branch of solutions (*b*) begins at the first limit point and ends at the secondary limit point; along this branch the incoming swirl is reduced. Solutions along the fold describe a swirling flow with a localized standing wave that develops into a localized separation zone as the swirl approaches the secondary limit point. The branch of solutions (*c*) starts from the secondary limit point; along that branch the incoming swirl is increased and solutions describe a large separation zone. Beran & Culick (1992) indicated that there may be a possible relation between the first limit point in their computations and the critical swirl as defined by Benjamin (1962). They also conducted numerical computations using the quasi-cylindrical approximation of Hall (1967) and found a singular behaviour as the swirl approaches the first limit point.

More recently, Lopez (1994) and Beran (1994) studied the solutions of the unsteady axisymmetric Navier–Stokes equations. Both of these analyses showed that the aforementioned branches of solutions (*a*) and (*c*) are stable to small axisymmetric disturbances, whereas the solutions along (*b*), in the fold, are unstable. Steady-state solutions along the branch (*b*) cannot develop in a dynamical process starting from any initial swirling flow. Moreover, starting from solutions along the fold the flow may evolve into one of the solutions along branches (*a*) or (*c*).

The stability analyses of rotating flows study the tendency of imposed small disturbances to grow or decay in time and space. The analyses of Rayleigh (1916), Howard & Gupta (1962), Lessen, Singh & Paillet (1974) and Leibovich & Stewartson (1983) defined several stability criteria relating to axisymmetric and general three-dimensional disturbances. It is found, for example, that a vortex with a large rotational core (the '*Q*-Vortex' model) is stable to axisymmetric perturbations when the swirl ratio is greater than 0.403, and is unstable to helical perturbations only when the swirl ratio is less than about 1.6. A review of vortex stability criteria is given in Leibovich (1984). It is important to note that the relation between vortex breakdown and vortex stability is yet unclear. Leibovich (1984) pointed out that breakdown can occur in a vortex flow with just a little sign of instability and a vortex flow can become unstable without any breakdown phenomenon.

The summary of theoretical studies as presented above and in figure 1 indicates that there may be a possible relation between the critical swirl of the inviscid theory and vortex breakdown. Specifically, the inviscid theories of Benjamin (1962), Leibovich & Kribus (1990) and Buntine & Saffman (1995) show some correlation with the viscous computations of Hall (1972) and Beran & Culick (1992). However, figure 1 demonstrates that large gaps still exist between the various theoretical approaches and the numerical computations. Specifically, the relation between the solutions of Leibovich & Kribus (1990) and the special solution of Keller *et al.* (1985) is not clear. Moreover, the steady-state inviscid analyses do not provide insight into the special behaviour of the numerical solutions of the axisymmetric Navier–Stokes equations of Beran & Culick (1992), Beran (1994) and Lopez (1994). The relation between

the critical swirl and the first limit point as suggested by Beran & Culick (1992) is not fully understood and there is no explanation for the existence of the secondary limit point that appears in the viscous computations. It should also be emphasized that none of the known stability analyses can shed any light on the specific stability characteristics of solutions of the axisymmetric Navier–Stokes equations as found in the numerical solutions of Beran (1994) and Lopez (1994).

The breakdown of vortex cores is a remarkable feature of swirling flows and is still a basic, largely unexplained, phenomenon. Although several explanations of vortex breakdown have been proposed, a consistent description of this complicated phenomenon has not yet been provided. Also, the relation between the various theoretical and numerical solutions is not completely clear. A theoretical approach that clarifies the physical mechanism leading to axisymmetric vortex breakdown and that provides the conditions for which the various solutions may appear in a numerical simulation or experiment has never been derived, and is of great scientific and technological importance.

The objective of this paper is to present a new study of the axisymmetric vortex breakdown phenomenon. Our approach is based on a thorough investigation of the dynamics of an axisymmetric swirling flow in a finite-length constant-area pipe as described by the axisymmetric unsteady Euler equations (§1.2). We consider certain boundary conditions that may reflect the physical situation. Along the pipe inlet we specify for all time the axial and circumferential velocity components as well as the azimuthal vorticity. We allow the inlet flow a degree of freedom to develop a radial velocity, to reflect the upstream influence by disturbances that have the tendency to cast such an influence. Along the pipe outlet we pose a no-radial-flow state. We also consider an initial state that describes a perturbed columnar flow along the pipe. We study the stability characteristics as well as the time-asymptotic behaviour as it is related to the steady-state solutions. The results are established through a rigorous mathematical analysis and provide a solid theoretical understanding of the dynamics of an axisymmetric swirling flow in a pipe.

The inlet conditions described above reflect a specific vortex state. In the physical situation this vortex state is generated by a certain device and the mechanism of the vortex generation is always due to strong viscous effects. On the other hand, the mechanism leading to vortex breakdown in high-Reynolds-number flows is believed to be related mainly to inviscid effects. Therefore, a proper theoretical approach to study the problem may separate the two issues. In this paper we concentrate on the vortex breakdown problem. The interaction between the vortex generator and the vortex breakdown phenomenon should be considered in a future study.

In this study we specify the vortex state at the pipe inlet. This condition may provide a realistic approximation of the flow state at the exit of a vortex generator (see, for example, the experimental results of Bruecker & Althaus 1995). In most of the experimental apparatuses a slightly diverging pipe was used to promote the appearance of the breakdown phenomena by creating an adverse pressure gradient. The slightly diverging pipe does not allow disturbances in the flow to propagate upstream and change the inlet conditions. Our inlet conditions may reflect the physics of such a case even though a straight pipe is used. The relation between the slightly diverging pipe case and the straight pipe case can be established using the same analysis methods as described in this paper.

It should also be noticed here that the numerical simulations by Salas & Kuruvila (1989), Beran & Culick (1990), Lopez (1994), Beran (1994) and Darmofal (1996) and some of the theoretical studies (Buntine & Saffman 1995) considered similar boundary

conditions to those used in this paper. A good correlation was found between the results of the axisymmetric simulations and the experimental data (see Darmofal 1996). These studies revealed the dynamics of swirling flows and the evolution of the axisymmetric vortex breakdown in a pipe and our theoretical results provide an explanation of these investigations.

We summarize here the main steps of the analysis. We first reveal the possible steady-state solutions that may develop as the swirl level of the incoming flow is increased from zero to above the critical level (see §§2–7 and Appendices A–D). This has been done by using a variational method to study the functional $\mathscr{E}(\psi(x, y))$ whose stationary points correspond to inviscid steady-state solutions (here, $\psi(x, y)$ is the stream function and $y = r^2/2$). In §2 we discuss the existence and properties of a steady-state solution which is the global minimizer of $\mathscr{E}(\psi(x, y))$ and show that this solution is strongly dominated by the global minimizer of the functional $E(\psi(y))$ which corresponds to the columnar (x-independent) problem. Therefore, in §3 we conduct a thorough study of the various solutions of the columnar problem. The results of §§2 and 3 are applied in §4 to describe in detail the global minimizer solutions of the steady Euler equations as the inlet swirl is increased.

In §5 we extend Benjamin's definition of the critical state to a columnar flow in a finite-length pipe. In §6 we show the existence of a branch of min-max solutions of $\mathscr{E}(\psi(x, y))$ that naturally appears. In §7 we present the global bifurcation diagram of solutions of the steady Euler equations based on the above results. The global bifurcation diagram also shows the relations between the various analyses of Benjamin (1962), Leibovich & Kribus (1990) and Keller *et al.* (1985) and demonstrates the correlation between the inviscid theory and the numerical simulations of high-Reynolds-number flows described by Beran & Culick (1992).

In §8 we summarize our recent results that revealed, for the first time, the special relation between the stability of swirling flows in a finite-length pipe and the critical swirl. We show that the critical swirl is a point of exchange of stability (see Wang & Rusak 1996*a, b*). We also show that the stability is closely related to the global bifurcation diagram of steady-state solutions. Moreover, the stability results provide a theoretical understanding of the specific stability characteristics as described in the numerical studies of the Navier–Stokes equations by Lopez (1994) and Beran (1994).

The stability analyses together with the study of steady-state solutions suggests a consistent explanation of the mechanism leading to axisymmetric vortex breakdown in high-Reynolds-number swirling flows in a pipe (§9). It is an evolution from an initial columnar swirling flow to another, relatively stable, equilibrium state which represents a flow around a separation zone. This evolution is the result of the loss of stability of the columnar base state when the swirl ratio of the incoming flow is near or above the critical level. The instabilty mechanism is governed by the interaction of disturbances propagating upstream with the inlet state. Our recent numerical computations, guided by the present theory (Rusak, Wang & Whiting 1996), demonstrate the relations between the stability of swirling flows and the critical swirl and provide the time history of the nonlinear transition.

Section 10 discusses the effects of slight viscosity on the development of a steady swirling flow and shows the relation between the present study and the numerical computations using the axisymmetric Navier–Stokes equations. We find that the present approach, based on the Euler equations, is the inviscid-limit theory of the axisymmetric viscous flow problem.

1.2. *Mathematical model*

1.2.1. *Basic problem*

An axisymmetric incompressible and inviscid swirling flow is considered in a finite-length pipe of unit radius ($0 \leqslant r \leqslant 1$) and length x_0 where $0 \leqslant x \leqslant x_0$. The axial and radial distances are rescaled with the radius of the pipe. Let $y = r^2/2$ where $0 \leqslant y \leqslant 1/2$. By virtue of the axisymmetry, a stream function $\psi(x, y, t)$ can be defined where the radial component of velocity $u = -\psi_x/(2y)^{1/2}$, and the axial component of velocity $w = \psi_y$. The equations which connect the development in time, t, of the stream function ψ, the azimuthal vorticity $\eta = r\chi$, where $\chi = -(\psi_{yy} + \psi_{xx}/2y)$, and the circulation function $K = rv$ (where v is the circumferential velocity) may be given by (see, for example, Szeri & Holmes 1988)

$$K_t + \{\psi, K\} = 0, \quad \chi_t + \{\psi, \chi\} = \frac{1}{4y^2}(K^2)_x. \tag{1}$$

Here the brackets $\{\psi, K\}$ and $\{\psi, \chi\}$ are defined by

$$\{\psi, K\} = \psi_y K_x - \psi_x K_y, \quad \{\psi, \chi\} = \psi_y \chi_x - \psi_x \chi_y. \tag{2}$$

We study the development of the flow with certain conditions posed on the boundaries. For any time, t, we set $\psi(x, 0, t) = 0$ to enforce axisymmetry along the pipe axis, and $\psi(x, 1/2, t) = \overline{w}_0$ which gives the total mass flux across the pipe. Along the inlet, $x = 0$, for any time, t, an incoming flow profile described by the axial flow, the circulation and the azimuthal vorticity is given as

$$\begin{rcases} \psi(0, y, t) = \psi_0(y), \quad K(0, y, t) = \omega K_0(y), \\ \chi(0, y, t) = -\psi_{0yy} \quad (\text{or} \quad \psi_{xx}(0, y, t) = 0). \end{rcases} \tag{3}$$

Here ω reflects the swirl level of the incoming flow. The radial velocity component along the inlet is found as part of the solution of the problem. We allow the inlet state a degree of freedom to develop a radial velocity, to reflect the upstream influence by disturbances that have the tendency to cast such an influence. Along the pipe outlet, $x = x_0$, we set the radial velocity component to zero, i.e.

$$\psi_x(x_0, y, t) = 0 \tag{4}$$

for all time. For a long straight pipe ($x_0 \gg 1$) this outlet condition only weakly affects the upstream flow. Similar boundary conditions have been considered by Salas & Kuruvila (1989), Beran & Culick (1990) and Lopez (1994) in their numerical simulations of the Navier–Stokes equations and by Buntine & Saffman (1995) in their theoretical study of a steady swirling flow in a finite-length diverging pipe using the Euler equations. These boundary conditions may also reflect the physical situation as reported in Bruecker & Althaus's (1995) experiments. We want to point out that in certain cases where the pipe is short and diverges significantly, such as in combustion chambers and the studies by Buntine & Saffman (1995), different outlet conditions may have a strong effect on the flow and result in different solutions.

The problem defined by equations (1)–(4) is well posed and describes the evolution of a swirling flow in a finite-length pipe. We consider some relevant initial conditions for the stream function, circulation and azimuthal vorticity, such as a perturbed columnar state throughout the pipe at $t = 0$

$$\begin{rcases} \psi(x, y, 0) = \psi_0(y) + \epsilon_\psi(x, y), \quad K(x, y, 0) = \omega K_0(y) + \epsilon_K(x, y), \\ \chi(x, y, 0) = -\psi_{0yy} - \epsilon_\chi(x, y) \end{rcases} \tag{5}$$

where $\epsilon_\psi(x, y), \epsilon_K(x, y)$ and $\epsilon_\chi(x, y)$ are prescribed disturbances. Here,

$$\psi(x, y, t) = \psi_0(y), \quad K(x, y, t) = \omega K_0(y), \quad \chi(x, y, t) = -\psi_{0yy}$$

is a base steady-state solution of (1)–(4) for any time t and every swirl level, ω, that describes a columnar flow. Starting from the initial conditions (5), it is expected that the flow will develop uniquely in time. Drazin & Howard (1966) proved the uniqueness of a time-dependent solution of the Euler equations for similar boundary conditions and any initial state. Also, we believe that the axisymmetric vortex breakdown is primarily related to the swirl level, ω, of the incoming flow. Therefore, we fix the functions $\psi_0(y)$ and $K_0(y)$ and look for different solutions of (1)–(5) for various levels of ω.

In order to understand the dynamics of a swirling flow governed by (1) with boundary conditions (3) and (4) and initial conditions (5), it is important to study the stability characteristics and the time-asymptotic behaviour, specifically as it is related to steady-state solutions of the problem. We will first concentrate on the analysis of the steady-state solutions of these equations for a given swirl level, ω, and prove the existence of multiple steady-state solutions of the problem (1)–(4). We will derive the bifurcation diagram of steady-state solutions as the swirl level, ω, of the incoming flow is changed. The bifurcation diagram resulting from our analysis is summarized in §7. In §8 we will return to study the dynamics of a swirling flow governed by (1)–(5). We will examine the linear stability of the various steady-state solutions found in our analysis according to the recently presented results by Wang & Rusak (1996*a, b*). The bifurcation diagram of steady-state solutions together with the stability results will shed new light on the evolution of swirling flows as described by (1)–(5) (see §9).

1.2.2. *Steady-state problem*

When the flow is steady equations (1)–(4) may be reduced to the Squire–Long equation (SLE) (Squire 1956 and Long 1953, also known as the Bragg–Hawthorne 1950 equation):

$$\psi_{yy} + \frac{\psi_{xx}}{2y} = H'(\psi) - \frac{I'(\psi)}{2y} \qquad \text{on} \quad \Omega_{x_0} = (0, x_0) \times (0, 1/2) \tag{6}$$

with boundary conditions

$$\left. \begin{array}{c} \psi(x, 0) = 0, \quad \psi(x, 1/2) = \overline{w}_0, \\ \psi(0, y) = \psi_0(y), \quad K(0, y) = \omega K_0(y), \quad \psi_{xx}(0, y) = 0, \quad \psi_x(x_0, y) = 0 \end{array} \right\} \tag{7}$$

Here, H is the total head function, $H = p/\rho + (u^2 + w^2 + v^2)/2$, p is the static pressure and ρ is the density. $I = K^2/2$ is the extended circulation function. H and I are conserved along a streamline and, therefore, are functions of ψ only. These functions may be determined from the inlet profiles $\psi_0(y)$, $K_0(y)$ and the swirl level ω. Therefore, the columnar vortex flow $\psi(x, y) = \psi_0(y)$, $K(x, y) = \omega K_0(y)$ is a base solution of (6) and (7) for any swirl level ω. For relevant inlet flows such as the Rankine vortex, the Burgers' vortex or the 'Q-vortex', it can be shown that both H and I are nonlinear functions of ψ (see, for example, figure 2 and (21) and (22) below); H is approximately a linear function of ψ and I is approximately a quadratic function for small ψ, and both are almost constant when ψ is near $\overline{w}_0 = \psi_0(1/2)$. This nonlinearity may give rise to multiple solutions of (6) and (7) for a fixed value of ω, in addition to the base solution.
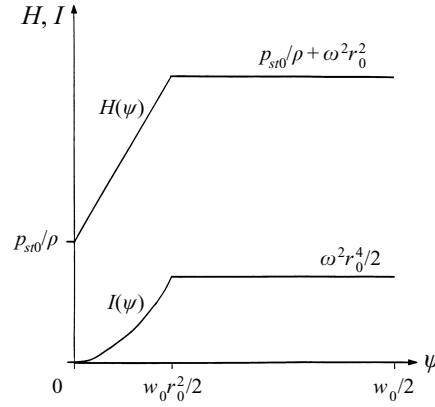
FIGURE 2. The total head and circulation functions for the Rankine vortex (see (21) and (22)).

It should be noticed, however, that for certain cases relevant to vortex breakdown, the flow may evolve uniquely in time from an initial near-columnar state to a steady state that contains a separation zone. From the perspective of the steady-state problem, the specification of the functions H and I inside the separation zone is problematic. However, from the perspective of the time-dependent problem described above, the determination of the functions H and I in the separation zones should depend on the time-history of the flow starting from initial conditions (5). We will study in this paper various possible continuation models of the functions H and I in the separation zone and describe the resulting steady-state solution from those models. We will relate these various possible steady-state solutions to the expected (unique) behaviour of the solution of the time-dependent Euler equations (1)–(4) with initial conditions (5). Using this idea, we will suggest describing the separation region as a stagnation zone, where the flow inside this zone evolves in time from a flow region concentrated around the centreline at the pipe inlet. Physical considerations and numerical simulations of inviscid and unsteady swirling flows (see Rusak *et al.* 1996) also demonstrate that the stagnation model is a relevant model to describe the functions H and I in the separation zone.

Solutions of (6) are well known to correspond to the stationary points of the following functional:

$$\mathscr{E}(\psi) = \int_0^{x_0} \int_0^{1/2} \left(\frac{\psi_y^2}{2} + \frac{\psi_x^2}{4y} + H(\psi) - \frac{I(\psi)}{2y} \right) \mathrm{d}y\mathrm{d}x. \tag{8}$$

This variational principle was first introduced into the study of vortex breakdown by Benjamin (1962) and was also used by Keller *et al.* (1985). We find that for various values of ω, the functional $\mathscr{E}(\psi)$ has a complicated behaviour due to the nonlinear nature of $H(\psi)$ and $I(\psi)$. The study of this behaviour will help to identify the various solutions of (6) and (7) for a given ω. As we will show, some of the solutions of the SLE do not bifurcate immediately from the base columnar flow solution mentioned above and, therefore, cannot be detected by a local asymptotic analysis. Consequently, a global analysis of $\mathscr{E}(\psi)$ and a rigorous mathematical study is essential and will shed light on the development of a swirling flow in a pipe.

2. Global minimizer of $\mathcal{E}(\psi)$

2.1. Existence of global minimizer of $\mathcal{E}(\psi)$

The natural step in the variational analysis is to seek the minimizer of $\mathcal{E}(\psi)$. We rigorously prove (see Appendix A, Theorem A.1) that the global minimizer solution $\psi_g(x, y)$ of $\mathcal{E}(\psi)$ exists under the conditions:

1. $H(\psi)$ and $I(\psi)$ are bounded and piecewise smooth non-negative functions with bounded first derivatives;

2. $I(\psi) \leqslant c|\psi|^p$ where p is a fixed number, $1 < p \leqslant 2$, and $c > 0$.

The boundedness of both $H(\psi)$ and $I(\psi)$ does not limit our approach since we are interested in solutions with bounded mechanical energy and circulation coming into the pipe. It should also be clarified that if assumption 1 is not satisfied it can be shown that the global minimizer of $\mathcal{E}(\psi)$ may not exist.

We also show in Appendix A that the global minimizer solution is a regular solution such that its first derivatives are continuous everywhere. It should be pointed out that this solution of the SLE, (6) and (7), may allow discontinuous second derivatives but it is nonetheless a solution of the steady Euler equations. Moreover, as we later claim, in relevant cases a near columnar flow state may evolve naturally, in infinite time, into the flow state described by the global minimizer solution with discontinuous second derivatives. We find in this paper that, for certain values of ω, specifically for high swirl cases, the global minimizer of $\mathcal{E}(\psi)$ is not the base columnar flow solution $\psi(x, y) = \psi_0(y)$ and another solution that describes a different flow state is the global minimizer of $\mathcal{E}(\psi)$.

In §2.2, we turn to the study of the columnar flow problem of (6) and (7), and the behaviour of the columnar minimizers. In §2.3, we show the special relations between the global minimizer $\psi_g(x, y)$ of $\mathcal{E}(\psi)$ and the global minimizer of the columnar problem.

2.2. Columnar flow

In the case of a columnar swirling flow where $\psi_x \equiv 0$ everywhere in Ω_{x_0}, equation (6) is reduced to the ordinary differential equation

$$\psi_{yy} = H'(\psi) - \frac{I'(\psi)}{2y} \tag{9}$$

with boundary conditions

$$\psi(0) = 0, \ \psi(1/2) = w_0. \tag{10}$$

Here the stream function ψ is a function of y only. The corresponding variational principle is

$$E(\psi) = \int_0^{1/2} \left(\frac{\psi_y^2}{2} + H(\psi) - \frac{I(\psi)}{2y} \right) dy. \tag{11}$$

It can be shown that for any solution of (9), $E(\psi) = \int_0^{1/2} (p/\rho + w^2) dy$, which represents the flow force of the columnar flow in a pipe (Benjamin 1962).

We can prove from an argument similar to that in Appendix A, that the minimizer of the columnar functional $E(\psi)$ exists for given $H(\psi)$ and $I(\psi)$ that satisfy the same assumptions in Theorem A.1. Let $\psi_s(y)$ denote the global minimizer of the columnar functional $E(\psi)$.
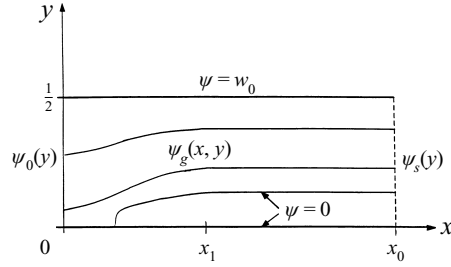
FIGURE 3. A schematic description of the global minimizer solution $\psi_g(x, y)$.

2.3. *Properties of the global minimizer of $\mathscr{E}(\psi)$*

We prove in Appendix B the relation between $\psi_g(x, y)$, the global minimizer of $\mathscr{E}(\psi)$, and $\psi_s(y)$, the global minimizer of the columnar functional $E(\psi)$ with the same functions $H(\psi)$ and $I(\psi)$. We show that the outlet state of the global minimizer solution, $\psi_g(x_0, y)$, tends to the columnar global minimizer solution, $\psi_s(y)$, as the length of the pipe x_0 is increased. This means that the global minimizer of the PDE, (6) and (7), is controlled by the minimizer of the columnar problem (9) and (10). The global minimizer $\psi_g(x, y)$ describes a transition along the pipe from the inlet state $\psi_0(y)$ to the state $\psi_s(y)$ along the outlet (see figure 3).

This result is quite natural once we notice that the global minimizer of the columnar problem is not subjected to the inlet conditions. In certain cases, specifically when the swirl level is high, $\psi_s(y)$ may not be the state $\psi_0(y)$ which means that $E(\psi_s(y)) < E(\psi_0(y))$. Therefore, in order to minimize $\mathscr{E}(\psi)$ the global minimizer $\psi_g(x, y)$ describes a spatial transition with a minimal contribution to $\mathscr{E}(\psi)$ from the inlet state $\psi_0(y)$ to the state $\psi_s(y)$. When the pipe length x_0 is long we can show that the length x_1 of this transition is finite where $x_1 < x_0$ and in the range $x_1 < x < x_0$ the global minimizer $\psi_g(x, y)$ is very close to the columnar state given by $\psi_s(y)$ (see figure 3).

2.4. *Balance of flow force*

Multiplying (6) by ψ_x on both sides and integrating, we find

$$\int_0^{\tilde{x}} \int_0^{1/2} \left(\psi_{yy}\psi_x + \frac{\psi_{xx}\psi_x}{2y} \right) dy dx = \int_0^{1/2} dy \int_0^{\tilde{x}} \left(H'(\psi)\psi_x - \frac{I'(\psi)}{2y}\psi_x \right) dx.$$

Integration by parts and the use of boundary conditions gives

$$-\int_0^{1/2} dy \int_0^{\tilde{x}} d\left(\frac{\psi_y^2}{2} \right) + \int_0^{1/2} \frac{\psi_x^2(\tilde{x}, y) - \psi_x^2(0, y)}{4y} dy$$

$$= \int_0^{1/2} \left(H(\psi(\tilde{x}, y)) - \frac{I(\psi(\tilde{x}, y))}{2y} \right) dy - \int_0^{1/2} \left(H(\psi(0, y)) - \frac{I(\psi(0, y))}{2y} \right) dy. \quad (12)$$

We define the function

$$S(x) = \int_0^{1/2} \left(\frac{\psi_y^2(x, y)}{2} - \frac{\psi_x^2(x, y)}{4y} + H(\psi(x, y)) - \frac{I(\psi(x, y))}{2y} \right) dy$$

$$= E(\psi(x, y)) - \int_0^{1/2} \frac{\psi_x^2(x, y)}{4y} dy. \quad (13)$$

Here, $E(\psi(x, y))$ is calculated at a fixed cross-section x using (11). Then, for any solution of (6), we can rewrite (12) as

$$S(x) = \text{constant} = S(0) \quad \text{for all} \ \ 0 \leqslant x \leqslant x_0. \tag{14}$$

We can show that $S(0) = \int_0^{1/2} (p/\rho + w^2)_{x=0} \mathrm{d}y$. The function $S(x)$ is the 'flow force' that must be constant at any cross-section x along the straight pipe due to the conservation of the axial momentum. From the boundary conditions (7), we may find that for any solution, $\psi(x, y)$, of the problem given by (6) and (7),

$$E(\psi_0(y)) - E(\psi(x_0, y)) = \int_0^{1/2} \frac{\psi_x^2(0, y)}{4y} \mathrm{d}y \geqslant 0. \tag{15}$$

This means that for a steady-state solution of (6) and (7) we have $E(\psi_0(y)) \geqslant E(\psi(x_0, y))$. Specifically, for the global minimizer $\psi_g(x, y)$ of $\mathscr{E}(\psi)$, where x_0 is large, we find

$$E(\psi_0) - E(\psi_s) = \int_0^{1/2} \frac{\psi_{gx}^2(0, y)}{4y} \mathrm{d}y \geqslant 0. \tag{16}$$

In the case where the global minimizer solution of the columnar problem, $\psi_s(y)$, is different from the inlet state $\psi_0(y)$, we have $E(\psi_s) < E(\psi_0)$. Since the global minimizer of the SLE describes a transition from the inlet state $\psi_0(y)$ to the outlet state $\psi_s(y)$, we can understand from (16) that the difference $E(\psi_0) - E(\psi_s)$ is related in this solution to the establishment of a radial velocity component along the inlet.

3. Study of columnar swirling flow

Sections 2.3 and 2.4 raise the need to study the solutions of the columnar problem, (9) and (10), in order to identify global minimizer solutions of (6) and (7) at various levels of swirl.

In the theoretical studies of vortex breakdown, the inlet flow, $\psi_0(y)$ and $K_0(y)$, was commonly approximated by one of the following models: the Rankine vortex (Keller *et al.* 1985), the Burgers vortex (Leibovich & Kribus 1990) and the Q-vortex model (Leibovich 1984). Each of these vortex models is characterized by a swirl parameter ω. It can be shown that in each case there exists a critical swirl level, ω_B, as defined by Benjamin (1962), that can be determined by the following eigenvalue problem derived from the linearized SLE (9) and (10):

$$\left. \begin{aligned} \phi_{yy} - \left(H''(\psi_0; \omega_B) - \omega_B^2 \frac{\tilde{I}''(\psi_0)}{2y} \right) \phi = 0, \\ \phi(0) = \phi(1/2) = 0. \end{aligned} \right\} \tag{17}$$

Here $\tilde{I} = K_0^2/2$. Benjamin (1962) classified a columnar vortex as supercritical, critical or subcritical according to $\omega < \omega_B$, $\omega = \omega_B$ and $\omega > \omega_B$, respectively. Benjamin's classification is related to the dynamics of small-disturbance waves in the base swirling flow. Supercritical flows have a low swirl ratio and are unable to sustain axisymmetric small-disturbance standing waves. Subcritical flows have a high swirl ratio and are able to support such waves. At the critical state, an infinitely long small-disturbance standing wave may develop.

From the perspective of variational methods it can be shown (see for example Courant & Hilbert 1953) that supercritical states (where $\omega < \omega_B$) are local minimizers of the functional $E(\psi)$.

In the rest of this paper, we concentrate on the case where the inlet profile $\psi_0(y)$ is modelled by either the Rankine or the Burgers vortex. These are used as basic analysis models to develop our new approach because of their analytical simplicity. However, the results shown in this paper can also be extended to other relevant vortex model (see our recent results on a Q-vortex in Rusak, Whiting & Wang 1997).

3.1. *The Rankine vortex*

The Rankine vortex is defined as a vortex flow with uniform axial velocity

$$w = w_0 \tag{18}$$

and swirl component

$$v = \begin{cases} \omega r, & 0 \leqslant r \leqslant r_0, \\ \omega r_0^2/r, & r_0 \leqslant r \leqslant 1. \end{cases} \tag{19}$$

For a columnar state the pressure is given by

$$\frac{\mathrm{d}p}{\mathrm{d}r} = \rho \frac{v^2}{r}. \tag{20}$$

Here ω is the angular speed at the centre and r_0 is the vortex core size. The functions $H(\psi)$ and $I(\psi)$ are calculated from (18)–(20) as (see figure 2)

$$H(\psi) = \begin{cases} p_{st0}/\rho + (2\omega^2/w_0)\psi & \text{when } 0 \leqslant \psi \leqslant \frac{1}{2}w_0 r_0^2, \\ p_{st0}/\rho + \omega^2 r_0^2 & \text{when } \frac{1}{2}w_0 r_0^2 \leqslant \psi \leqslant \frac{1}{2}w_0 \end{cases} \tag{21}$$

and

$$I(\psi) = \begin{cases} (2\omega^2/w_0^2)\psi^2 & \text{when } 0 \leqslant \psi \leqslant \frac{1}{2}w_0 r_0^2, \\ \frac{1}{2}\omega^2 r_0^4 & \text{when } \frac{1}{2}w_0 r_0^2 \leqslant \psi \leqslant \frac{1}{2}w_0. \end{cases} \tag{22}$$

Here p_{st0} is the total head at the centre, $p_{st0} = p_0 + \frac{1}{2}\rho w_0^2$ (where p_0 is static pressure at the centre).

The stream function for the Rankine vortex has a simple form:

$$\psi_0(y) = \psi_R(y) = w_0 y \tag{23}$$

which is a solution of (9) with boundary conditions (10) for $H(\psi)$ and $I(\psi)$ given by (21) and (22). Numerical solutions of the critical swirl ω_B as a function of the core radius r_0 are given in Keller *et al.* (1985) for the Rankine vortex. It is found, for example, that $2r_0\omega_B/w_0 = 2.405$ when r_0 is small. When $\omega < \omega_B, \psi_R = w_0 y$ describes a supercritical state and is a local minimizer of $E(\psi)$. In the following, we develop the behaviour of $E(\psi)$ for the Rankine vortex as ω increases from 0 to ω_B with r_0 and w_0 fixed.

Consider the special case $\omega = 0$. $E(\psi)$ is reduced in this case to

$$\left. \begin{array}{l} E(\psi) = \displaystyle\int_0^{1/2} \frac{\psi_y^2}{2}\mathrm{d}y, \\ \psi(0) = 0, \ \psi(1/2) = w_0/2. \end{array} \right\} \tag{24}$$

This is a strictly convex functional (see figure 4*a*) and the only stationary point of $E(\psi)$ is $\psi_R(y)$ which is a global minimizer of $E(\psi)$. When ω increases but is still small, $E(\psi)$ remains convex and $\psi_R(y)$ remains the global minimizer of $E(\psi)$.

We will show now that when ω becomes larger, but is still less than ω_B (in the
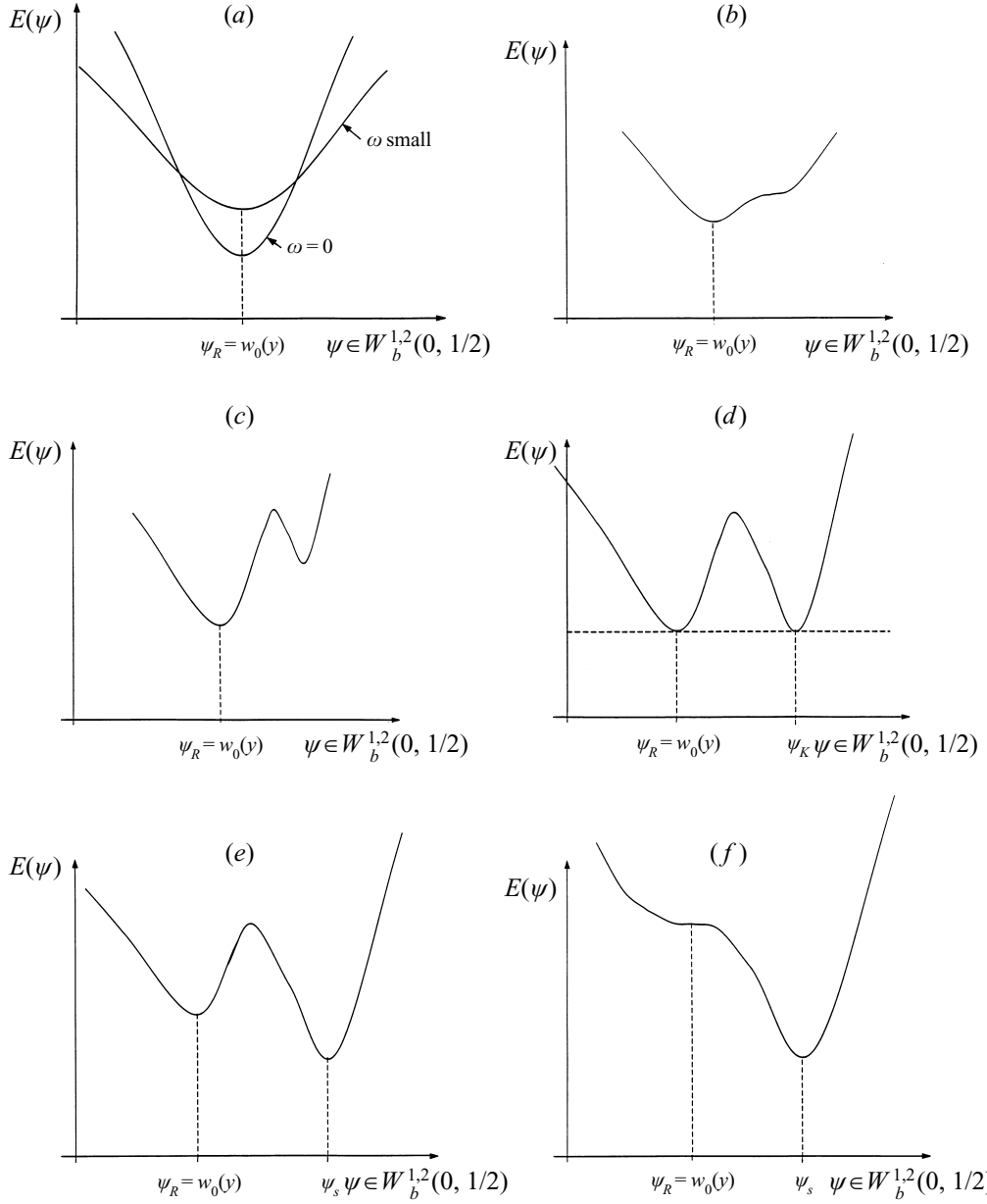
S. Wang and Z. Rusak

FIGURE 4. The functional $E(\psi)$ for (a) $\omega > 0$ but small, (b) $\omega = \omega^*$, (c) $\omega^* < \omega < \omega_0$, (d) $\omega = \omega_0$, (e) $\omega_0 < \omega < \omega_1$, (f) $\omega = \omega_B$.

supercritical region), $\psi_R(y)$ is no longer the global minimizer of $E(\psi)$. A calculation shows that

$$E(\psi_R) = \frac{p_{st0}}{2\rho} + \tfrac{1}{4}w_0^2 + \tfrac{1}{2}\omega^2 r_0^2 - \tfrac{3}{8}\omega^2 r_0^4 + \tfrac{1}{4}\omega^2 r_0^4 \ln(r_0^2). \tag{25}$$

We consider now the case where r_0 is small. Let

$$\psi_a = \begin{cases} 0, & 0 < y < a < \tfrac{1}{2}, \\ \tfrac{1}{2}w_0(y - a)/(\tfrac{1}{2} - a), & a < y < \tfrac{1}{2} \end{cases}$$
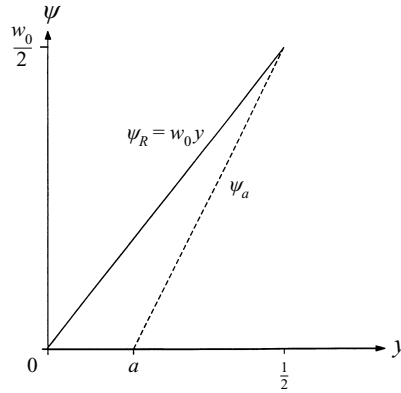
FIGURE 5. Stream function for the Rankine vortex and comparison function.

be a comparison function, which is not a solution of (9), see figure 5. Through a straightforward computation, we obtain for small r_0 and small a

$$E(\psi_a) = \frac{p_{st0}}{2\rho} + \frac{w_0^2}{8(\frac{1}{2} - a)} + \omega^2 r_0^2 (\frac{1}{2} - a) + O(\omega^2 r_0^4 \ln r_0).$$

Therefore,

$$E(\psi_R) - E(\psi_a) = -\frac{w_0^2 a}{4(\frac{1}{2} - a)} + \omega^2 r_0^2 a + O(\omega^2 r_0^4 \ln r_0).$$

For a small r_0 and a small $a > 0$, $E(\psi_R) > E(\psi_a)$ when

$$\omega > \frac{w_0}{\sqrt{2} r_0}. \tag{26}$$

Therefore, for this range of ω, $\psi_R(y)$ is no longer the global minimizer of $E(\psi)$.

Also, notice the fact that when $r_0 \sim 0$, $2\omega_B r_0/w_0 = 2.405$ (Keller *et al.* 1985). Therefore, we find that in its supercritical region, the Rankine vortex, ψ_R, is no longer the global minimizer of $E(\psi)$ when $\sqrt{2} < 2\omega r_0/w_0 < 2.405$ and where $r_0 \sim 0$. Actually, the numerical results of Keller *et al.* (1985) based on a stagnation model in the separation zone show that for the Rankine vortex, there exists a special swirl, ω_0, for any core size r_0, for which another solution, $\psi_K(y)$, of the columnar problem (9) and (10) is found. This special solution has the same flow force as $\psi_R(y)$, i.e. $E(\psi_R) = E(\psi_K)$. Figure 11 in Keller *et al.* (1985) gives the details of the solution for the special swirl ω_0 for any core size r_0. It is important to see that for every r_0 the swirl parameter ω_0 satisfies $0 < \omega_0 < \omega_1$. We can also see from their results that the estimate given in (26) for small r_0 is accurate.

From our viewpoint, ω_0 is a special swirl level because at ω_0 there exist two local minimizers of $E(\psi)$, $\psi_R(y)$ and $\psi_K(y)$, which have the same value of $E(\psi)$ (see figure 4*d*).

As ω increases above ω_0, $\psi_R(y)$ ceases to be a global minimizer of $E(\psi)$ and another global minimizer of $E(\psi)$ appears (see figure 4*e*). The new global minimizer describes a flow state that is very different from the Rankine vortex and will be shown in §3.2 to describe a separation zone in a swirling columnar flow.

Based on these arguments we can now summarize the behaviour of $E(\psi)$ as ω is increased (see figures 4*a–f*). In each figure ω is fixed.

(*a*) When ω is small the functional $E(\psi)$ has a unique stationary point, $\psi_R(y)$, which is the global minimizer of $E(\psi)$, see figure 4*a*.

(*b*) There exists a swirl level, ω^*, where two solutions are found, one is $\psi_R(y)$ and the other is different from $\psi_R(y)$. ω^* is actually a bifurcation point of the ODE problem (9) and (10). See figure 4*b*.

(*c*) When $\omega^* < \omega < \omega_0$, we find that $\psi = \psi_R(y)$ is still the global minimizer of $E(\psi)$, but two other stationary points can also be found. One is a local minimizer and the other is a min-max point of $E(\psi)$. The behaviour of $E(\psi)$ in this case is given in figure 4*c*.

(*d*) When $\omega = \omega_0$, the solution $\psi_K(y)$ obtained by Keller *et al.* (1985) is found, and $E(\psi)$ is shown in figure 4*d*. ω_0 is a threshold value of the swirl, across which the columnar global minimizer, $\psi_s(y)$, drastically changes.

(*e*) When $\omega > \omega_0$, we find that $\psi_R(y)$ is not a global minimizer of $E(\psi)$ since there exists a solution, $\psi_s(y)$, different from $\psi_R(y)$, for which $E(\psi_R) > E(\psi_s)$. The behaviour of $E(\psi)$ in this case is described in figure 4*e*.

(*f*) When $\omega = \omega_B$ (Benjamin's critical state), $\psi_R(y)$ is actually an inflection point of $E(\psi)$ along a special direction, and is no longer a local minimizer. The behaviour of $E(\psi)$ in this case is given in figure 4*f*.

The behaviour of $E(\psi)$ as described in figure 4 can be confirmed by numerical computations (see Rusak *et al.* 1996). Specifically, the existence of the special swirl levels ω^*, ω_0 and ω_B and multiple solutions when $\omega \geqslant \omega^*$ can be verified. Then, $E(\psi)$ for each solution can be calculated and compared one with the other to reveal the nature of each solution (local minimizer, global minimizer or min-max points of $E(\psi)$).

3.2. *The properties of ψ_s when $\omega > \omega_0$*

We have shown above that the columnar global minimizer $\psi_s = \psi_R(y)$ when $\omega < \omega_0$. However, when $\omega > \omega_0$, $\psi_s \neq \psi_R(y)$. In this section we study the properties of the global minimizer, ψ_s, of the columnar functional $E(\psi)$ when $\omega > \omega_0$. As we have seen in §2, these properties are essential to understand the qualitative behaviour of the global minimizer $\psi_g(x, y)$ of the axisymmetric functional $\mathscr{E}(\psi)$.

Let us consider all the solutions of (9) and (10) with $H(\psi)$ and $I(\psi)$ given by (21) and (22) which satisfy the condition $0 < \psi(y) < w_0$ for $0 < y < 1/2$. This condition is used here since the information that we have about the functions $H(\psi)$ and $I(\psi)$ according to (21) and (22) is limited to the range $0 < \psi(y) < w_0$. This condition results in solutions describing columnar flow states without separation zones. The family of these solutions may be given by

$$\psi_{r_c} = \begin{cases} \frac{1}{2}w_0\left(2y + (r_0^2 - r_c^2)\dfrac{(2y)^{1/2}}{r_c}\dfrac{J_1(2\omega(2y)^{1/2}/w_0)}{J_1(2\omega r_c/w_0)}\right) & \text{for } 0 < y < \tfrac{1}{2}r_c^2, 0 < \psi_{r_c} < \tfrac{1}{2}w_0 r_0^2, \\ w_0\dfrac{1-r_0^2}{1-r_c^2}(y - \tfrac{1}{2}r_c^2) + \tfrac{1}{2}w_0 r_0^2 & \text{for } \tfrac{1}{2}r_c^2 < y < 1/2, \end{cases}$$

(27)

where J_1 denotes the Bessel function of the first kind, r_0 is the Rankine vortex core radius and $r_c < 1$ is the vortical core radius of the solution ψ_{r_c}. The core size, r_c, is determined by the matching of axial velocity at $r = r_c$:

$$(r_0^2 - r_c^2)\frac{\omega}{r_c}\frac{J_0(2\omega r_c/w_0)}{J_1(2\omega r_c/w_0)} = -\frac{w_0(r_0^2 - r_c^2)}{1 - r_c^2}$$

(28)

where J_0 is the Bessel function of order zero. We see that $r_c = r_0$ is a trivial solution of

(28). There are also infinitely many non-trivial solutions of (28), $r_{c1} < r_{c2} < r_{c3} < ....$ However, analysis shows that all the solutions corresponding to $r_{c2}, r_{c3}, ...$ (except for r_{c1}) give values of $\psi_{r_c}(y)$ at some $0 < y < \frac{1}{2}r_c^2$ that are beyond the range $0 < \psi_{r_c}(y) < w_0$.

Direct computation using (27) and (28) shows that

$$E(\psi_{r_c}) = \frac{p_{st0}}{2\rho} + \tfrac{1}{4}w_0^2 + \omega^2(\tfrac{1}{8}r_c^4 + \tfrac{1}{2}r_0^2(1 - r_c^2) + \tfrac{1}{4}r_0^4\ln(r_c^2)). \tag{29}$$

Let $\psi_{r_{c1}}$ be the solution corresponding to r_{c1}; we have from (25) and (29)

$$E(\psi_{r_{c1}}) - E(\psi_R) = \frac{\omega^2 r_0^4}{8}\left(\frac{(r_{c1}^2 - r_0^2)(r_{c1}^2 - 3r_0^2)}{r_0^4} + 4\ln\left(\frac{r_{c1}}{r_0}\right)\right) > 0, \quad \text{when } r_{c1} > r_0. \tag{30}$$

It can also be shown that $r_{c1} > r_0$ when $\omega < \omega_B$. Thus, we conclude from (30) that $\psi_{r_{c1}}$ cannot be a minimizer of $E(\psi)$ when $\omega < \omega_B$. Actually, $\psi_{r_{c1}}$ is a min-max point of $E(\psi)$. Therefore, when $\omega_0 < \omega < \omega_B$, the global minimizer $\psi_s(y)$ of $E(\psi)$ must be some function other than the functions $\psi_R(y)$ and $\psi_{r_{c1}}(y)$ and $\psi_s(y)$ must have values beyond the interval $(0, w_0)$. In particular, $\psi_s(y)$ may become zero or negative somewhere on $0 < y < 1/2$, which means that a separation region may appear in the columnar minimizer when $\omega > \omega_0$. Therefore, we need to specify the functions $H(\psi)$ and $I(\psi)$ for negative values of ψ (to describe the flow in the separation zone). From physical reasons, any such extension must keep $H(\psi)$ and $I(\psi)$ bounded and so, according to the existence theorem, the global minimizer ψ_s exists.

We now discuss the properties of the minimizer, $\psi_s(y)$, of $E(\psi)$ when a stagnation model is considered to describe the flow in the separation zone. We also consider other continuation models and their relation to the stagnation model. These results will be used in §4 to describe the properties of the global minimizer solution of the SLE that corresponds to each continuation model. Then, we will demonstrate that the stagnation model is strongly related to the expected (unique) behaviour of the solution to the time-dependent Euler equations (1)–(5) as time tends to infinity.

3.2.1. *Stagnation model*

For a stagnation continuation model, $H(\psi)$ and $I(\psi)$ are extended to $\psi < 0$ as

$$H(\psi) = H(0) \text{ and } I(\psi) = I(0) = 0 \quad \text{for } \psi < 0. \tag{31}$$

It can be shown that in this case the global minimizer solution of (9) and (10), $\psi_s(y)$, must satisfy $\psi_s(y) \geqslant 0$ for any y in the domain $0 < y < 1/2$. To show this, consider the case where $\psi_s(y)$ is negative in some interval (y_1, y_2) in $0 < y < 1/2$. According to the extension (31), in this interval, $\int_{y_1}^{y_2}(\psi_{sy}^2/2 + H(\psi) - I(\psi)/2y)\mathrm{d}y > 0$. Therefore, in order to minimize the contribution of this interval to $E(\psi)$, we must have $\psi_s = 0$ in the entire interval (y_1, y_2). From the previous arguments that no solution can be a minimizer of $E(\psi)$ if $\psi > 0$ everywhere in the domain $0 < y < 1/2$, we find that the minimizer solution $\psi_s(y)$ of $E(\psi)$ must have a finite stagnation region. Figure 6(a) shows the solution $\psi_s(y)$ for $\omega > \omega_0$, where in the interval $0 \geqslant y \geqslant y_0$, $\psi_s(y) \equiv 0$.

3.2.2. *Relation to other continuation models*

Other possible continuation models, with bounded functions $H(\psi)$ and $I(\psi)$, may have a global minimizer solution, $\psi_s(y)$, with negative values in the domain $0 < y < \tilde{y}_0$ (see figure 6b). Therefore, $\psi_s(y)$ may describe in such a case a columnar flow state with regions of flow reversals. An example of using such a continuation model in the
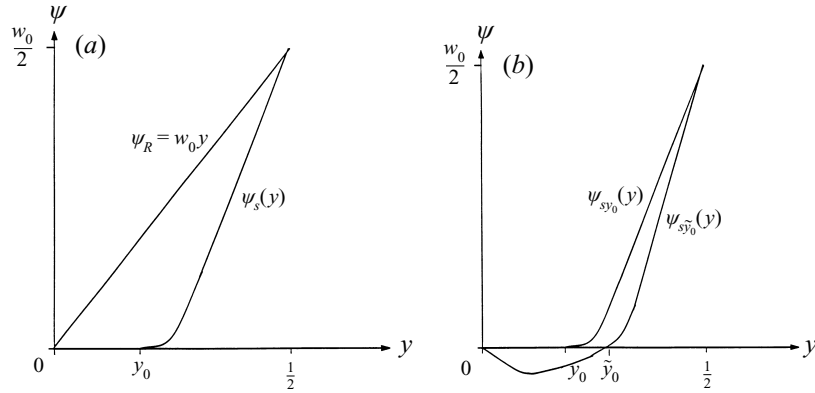
FIGURE 6. Stream functions, (*a*) for the columnar global minimizer when $\omega > \omega_0$ using a stagnation model in the separation zone, and (*b*) using a stagnation model in the separation zone and using another continuation model.

analysis of vortex breakdown is presented in Keller (1995). We argue that for a fixed level of swirl where $\omega \geqslant \omega_0$ we always have

$$\tilde{y}_0(\omega) \geqslant y_0(\omega), \tag{32}$$

i.e. for a fixed level of swirl the size of the separation zone is minimal when a stagnation model is used.

Comment: we will see in §4 that $\tilde{y}_0$ and y_0 are the characteristic sizes of the separation zones described by the global minimizer solutions, $\psi_g(x, y)$, of $\mathscr{E}(\psi)$ with the respective continuation models of $H(\psi)$ and $I(\psi)$.

To demonstrate (32), let us suppose that for a fixed level of swirl $\omega \geqslant \omega_0$ we have $\tilde{y}_0 < y_0$. We construct the following comparison function (see figure 6*b*)

$$\bar{\psi} = \begin{cases} \psi_{s\tilde{y}_0}, & 0 < y < \tilde{y}_0, \\ \psi_{sy_0}, & \tilde{y}_0 \leqslant y \leqslant 1/2. \end{cases} \tag{33}$$

Here, ψ_{sy_0} corresponds to the columnar minimizer calculated using the stagnation model and $\psi_{s\tilde{y}_0}$ corresponds to the columnar minimizer calculated for another continuation model. Then, we find that $E(\bar{\psi}) \leqslant E(\psi_{s\tilde{y}_0})$ and so $\bar{\psi}$ is also a minimizer of $E(\psi)$. But, as we notice from (33), there is a corner point in $\bar{\psi}$ at $y = \tilde{y}_0$, and this contradicts the regularity of the global minimizer solution (that is discussed in Appendix A).

We also notice that for other continuation models with bounded functions $H(\psi)$ and $I(\psi)$, the threshold value of swirl $\tilde{\omega}_0$ is always less than the value of ω_0 found in the case where a stagnation model is used. This result can also be seen in figure 3 of Keller (1995) for his special continuation model. To demonstrate this point, let ψ_{s0} be the solution at ω_0 when a stagnation model is used and let $\tilde{\psi}_{s0}$ be the solution at $\tilde{\omega}_0$ when another continuation model is used. Notice that according to the definition of ω_0 we have $E(\psi_{s0}; \omega_0) = E(\psi_R; \omega_0)$. Also, $E(\tilde{\psi}_{s0}; \omega_0) < E(\psi_{s0}; \omega_0)$. Therefore, $\tilde{\omega}_0$ must have a value that is less than ω_0 such that we can find $E(\tilde{\psi}_{s0}; \tilde{\omega}_0) = E(\psi_R; \tilde{\omega}_0)$.

3.3. *The Burgers vortex*

The discussion in this section helps to clarify the ideas developed above in §§3.1 and 3.2. The Burgers vortex is defined as a vortex flow with uniform axial velocity
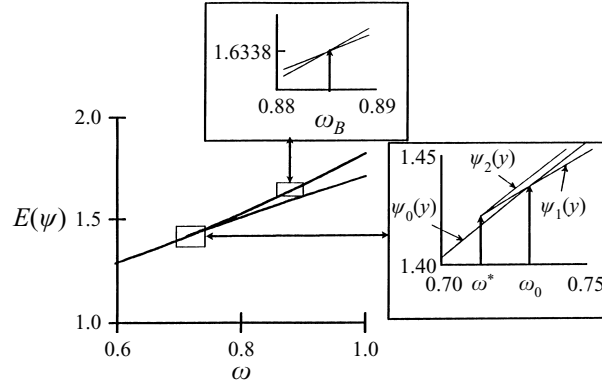
$$w = w_0 \tag{34}$$

FIGURE 7. Bifurcation diagram of solutions of the columnar problem for a Burgers vortex model
where $\beta = 1.0$ and $w_0 = 1.0$.

and swirl component

$$v = \omega \frac{(1 - e^{-\beta r^2})}{r} \tag{35}$$

or

$$\psi_0(y) = w_0 y, \quad K_0(y) = 1 - e^{-2\beta y}. \tag{36}$$

Here ω is the swirl level and β is related to the size of the vortical core, $r_c = 1.12/\beta^{1/2}$. The functions $H'(\psi)$ and $I'(\psi)$ are calculated from (34)–(36) as

$$H'(\psi) = w_0 \frac{I'(\psi)}{2\psi}, \quad I'(\psi) = \omega^2 \frac{2\beta}{w_0}(1 - e^{-2\beta\psi/w_0})e^{-2\beta\psi/w_0}. \tag{37}$$

Substituting (37) in (9) results in a nonlinear ODE for the solution of $\psi(y)$ with boundary conditions (10). Using the stagnation model described in (31), we solved (9) and (10) with (37) by standard numerical techniques. The results are presented in detail in Rusak *et al.* (1996) and we briefly summarize them in this section. A typical result where $w_0 = 1.0$ and $\beta = 4.0$ is presented in figure 7. We find that there exists a level of swirl ω^* which is a bifurcation point of solutions. When $\omega < \omega^*$ only the base flow solution $\psi = w_0 y$ exists. However, when $\omega = \omega^*$ two solutions exist: one is the base flow solution and the other is a special solution describing a swirling flow with a finite stagnation zone around the centreline. When $\omega > \omega^*$ three solutions are found: one is the base flow solution, $\psi_0(y)$, and the other two solutions $\psi_1(y)$ and $\psi_2(y)$ bifurcate from the non-trivial solution at ω^*. One of those, $\psi_1(y)$, describes a columnar state with a finite stagnation zone. As ω is increased above ω^* this branch of solutions describes a swirling flow state with a larger stagnation zone. Using equation (11) we calculated the flow force $E(\psi)$ for each solution and results are given in figure 7. We can see that there exists a level of swirl, ω_0, where $E(\psi_1) = E(\psi_0)$. For $w_0 = 1.0$ and $\beta = 4.0$ we find that $\omega_0 = 0.7305 < \omega_B = 0.8829$. When $\omega < \omega_0$ the base solution $\psi_0 = w_0 y$ is the global minimizer of $E(\psi)$, $\psi_s = \psi_0(y)$. However, when $\omega > \omega_0$ we find that the global minimizer of $E(\psi)$ is $\psi_s = \psi_1(y)$. These numerical calculations confirm the general behaviour of the bifurcation diagram as discussed in §3.1 for the Rankine vortex. For more details of these calculations see Rusak *et al.* (1996).

4. The properties of the global minimizer of $\mathscr{E}(\psi)$

In this section, the properties of the global minimizer $\psi_g(x, y)$ of $\mathscr{E}(\psi)$ (given by (8)) are examined. We will concentrate on the case where the inlet flow, $\psi_0(y)$, and $H(\psi)$ and $I(\psi)$ are described by the Rankine or Burgers vortex models. A similar discussion can be presented for other vortex models, such as the Q-vortex, and the qualitative results are expected to be the same. We discuss the nature of the global minimizer, $\psi_g(x, y)$, when a stagnation model is considered in the separation zone as well as other possible continuation models.

We distinguish between several cases as the swirl at the inlet is increased.

4.1. *The case where $0 < \omega \leqslant \omega_0$*

We will show first that when $0 \leqslant \omega \leqslant \omega_0$, the global minimizer of $\mathscr{E}(\psi)$ is the base columnar flow

$$\psi_g(x, y) \equiv \psi_0(y). \tag{38}$$

When $0 \leqslant \omega \leqslant \omega_0$, we have

$$
\begin{aligned}
\mathscr{E}(\psi) &= \int_0^{x_0} \int_0^{1/2} \left(\frac{\psi_y^2}{2} + H(\psi) - \frac{I(\psi)}{2y} \right) \mathrm{d}y\mathrm{d}x + \int_0^{x_0} \int_0^{1/2} \frac{\psi_x^2}{4y} \mathrm{d}y\mathrm{d}x \\
&\geqslant \int_0^{x_0} \int_0^{1/2} \left(\frac{\psi_{0y}^2}{2} + H(\psi_0) - \frac{I(\psi_0)}{2y} \right) \mathrm{d}y\mathrm{d}x + \int_0^{x_0} \int_0^{1/2} \frac{\psi_x^2}{4y} \mathrm{d}y\mathrm{d}x \\
&\geqslant \mathscr{E}(\psi_0)
\end{aligned}
\tag{39}
$$

and so (38) is proven. This result shows that in the range where $0 \leqslant \omega \leqslant \omega_0$, the inlet flow may develop all along the pipe as a columnar flow with no axial disturbance.

4.2. *The case where $\omega > \omega_0$*

The case where $\omega > \omega_0$ is more interesting. As is known from §3.1, the base flow state $\psi_0(y)$ is no longer a global minimizer of $E(\psi)$ in this range of ω and, therefore, the relation (39) does not hold in this case. The results of §2.3 and 2.4 can now be used to describe the properties of the global minimizer of $\mathscr{E}(\psi)$ when $\omega > \omega_0$.

We study two types of continuation models to describe the separation zone:

4.2.1. *Stagnation model*

(i) *ω slightly greater than ω_0*: In §2.3 we found that for a long pipe the global minimizer, $\psi_g(x, y)$, is dominated by the columnar minimizer $\psi_s(y)$. From §3, we also find that when ω is slightly greater than ω_0, the columnar minimizer, $\psi_s(y)$, is different from the inlet state, $\psi_0(y)$, and

$$E(\psi_0) - E(\psi_s) > 0 \quad \text{but small.} \tag{40}$$

From the boundary condition (4) and the momentum balance (16) we find that

$$E(\psi_0) - E(\psi_s) = \int_0^{1/2} \frac{\psi_{gx}^2(0, y)}{4y} \mathrm{d}y > 0 \quad \text{but small.}$$

The balance of flow force requires that the excess of E between inlet and outlet be converted into a relatively small radial flow along the inlet. Therefore, in the case where ω is slightly greater than ω_0, the global minimizer solution describes a transition from an inlet state that is almost the columnar state $\psi_0(y)$, to an outlet

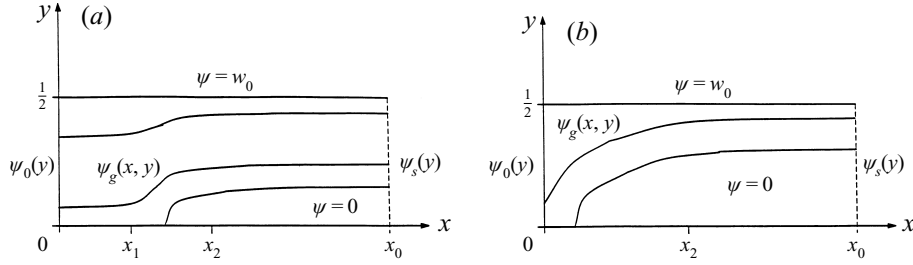FIGURE 8. The global minimizer solution $\psi_g(x, y)$ when $\omega > \omega_0$ and (a) ω close to ω_0, (b) $\omega - \omega_0$ is not small.

state that is the columnar flow $\psi_s(y)$, see figure (8a). Since the columnar minimizer, $\psi_s(y)$, must describe a separation zone (as shown in §3 for both the Rankine vortex model and the Burgers vortex model), the solution $\psi_g(x, y)$ describes the development of an open breakdown zone in the swirling flow.

The transition described by the global minimizer, $\psi_g(x, y)$, is composed of three flow stages along the pipe (see figure 8a). In the range $0 < x < x_1$, $\psi_g(x, y)$ is close to $\psi_0(y)$. In the range $x_1 < x < x_2$, $\psi_g(x, y)$ has a rather large radial flow component and the flow has a transition from $\psi_0(y)$ to $\psi_s(y)$. This transition must have the minimum of the functional $\mathscr{E}(\psi)$ among all the possible transitions. We may call it 'a minimum transition stage'. In the range $x_2 < x < x_0$, $\psi_g(x, y)$ is close to the columnar minimizer $\psi_s(y)$. Our numerical computations confirm this schematic description (see, for example, figure 8 in Rusak *et al.* 1996).

We can now see that when x_0 tends to infinity and $\omega \to \omega_0^+$ the global minimizer solution tends to the solution of Keller *et al.* (1985).

(ii) $\omega > \omega_0$, *and $\omega - \omega_0$ is not small*: In this case

$$\int_0^{1/2} \frac{\psi_{gx}^2(0, y)}{4y} \, \mathrm{d}y = E(\psi_g(0, y)) - E(\psi_g(x_0, y))$$

is not small. Thus, the radial velocity component $u(0, y)$ along the inlet ($u = -\psi_{gx}/(2y)^{1/2}$) is large, the open breakdown zone becomes larger and the breakdown position tends closer to the inlet, see figure 8(b). In this case, the global minimizer solution describes a relatively strong open breakdown. Our numerical computations also confirm this schematic description (see figure 9 and also Rusak *et al.* 1996 for more details).

4.2.2. *Other continuation models*

We first emphasize that according to the results in §§2 and 3 the global minimizer solution of the steady Euler equations, (6) and (7), must describe a swirling flow around an open separation zone when $\omega > \tilde{\omega}_0$. This solution cannot describe a swirling flow around a closed separation zone; and this fact is independent of the choice of continuation model. When continuation models, other than the stagnation model, are used we find global minimizer solutions that are similar to the solution described above, but with reversed flow in the open separation zone. Specifically, this means that the outlet section at $x = x_0$ becomes, partially, an inlet at the region where flow is reversed (see figure 10). The continuation model actually specifies the flow conditions at this inlet part at $x = x_0$. From the discussion in §3.2 we find that the separation zone becomes larger as ω is increased above $\tilde{\omega}_0$. Also, for each ω, the separation zone is larger than that described by the global minimizer
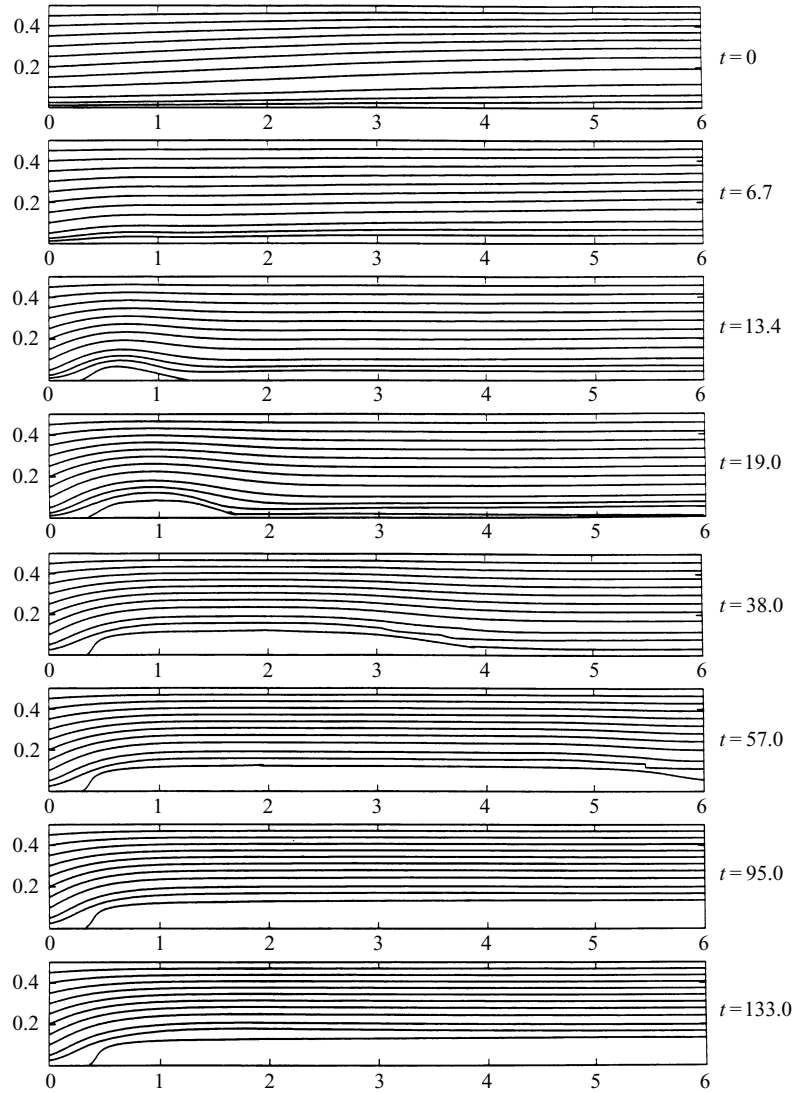
FIGURE 9. Time-history plots of the stream function for a pipe flow where the inlet state is described by the Burgers vortex model (34) and (35) and where $\omega = 1.0$ and $\beta = 4.0$. In these figures the top line is the pipe wall, the bottom line is the pipe centreline, the left section is the inlet and the right section is the outlet.

solution when a stagnation model is used. This shows that when reversed flow at $x = x_0$ enters the separation zone, the size of this zone becomes larger. This also shows that, within the inviscid and steady framework, different continuation models, that reflect different inlet conditions at part of the boundary at $x = x_0$, may result in different global minimizer solutions for every $\omega \geqslant \tilde{\omega}_0$. This demonstrates the non-uniqueness of solutions of the SLE (steady Euler equation) that may exist when various continuation models (various inlet conditions along part of the outlet) are used. In the inviscid and steady-state case, this non-uniqueness of solutions is expected, and within this framework, the choice of the proper model is an insoluble task. The various inviscid solutions may correspond to different physical situations,
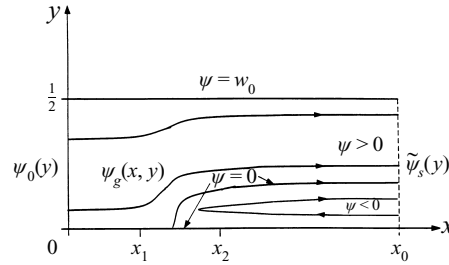
FIGURE 10. The global minimizer solution $\psi_g(x, y)$ when $\omega > \tilde{\omega}_0$ that corresponds to other continuation models.

not necessarily the physical situation that we look for in our case, i.e. the steady-state solution that may develop in time according to the unsteady Euler equations (1)–(5) as described in the mathematical model (§1). Starting from certain initial conditions of the flow in the pipe, the dynamics of the flow described by equations (1)–(5) leads naturally and uniquely to a certain steady-state solution which is related to only one specific model of continuation.

4.3. *Discussion on the global minimizer solution*

The above analysis shows that as the swirl of the incoming flow is changed around the level ω_0, the global minimizer solution drastically changes its nature from a columnar flow all along the pipe, when $\omega < \omega_0$, to a much different solution that must describe a swirling flow around an open breakdown zone, when $\omega > \omega_0$. The swirl level ω_0 is a turning point of the global minimizer solution.

In §4.2 we raised the problem of the choice of the continuation model in the separation zone to determine the global minimizer solution that is related to the dynamics of the flow as described by (1)–(5). We now discuss this dynamical process as presented in figure 9. Figure 9 represents a typical evolution of an inviscid swirling flow into a breakdown solution. Other cases given in Rusak *et al.* (1996) show a similar dynamical behaviour.

As we show later in this paper, the mechanism leading to vortex breakdown is the loss of stability of a subcritical swirling columnar flow. Therefore, when a columnar flow loses its stability, it must develop a radial velocity component which will result in a divergence of the streamlines near the centreline. This divergence becomes significant after some time and forms a large diverging region where the flow comes from the inlet flow concentrated near the centreline (figure 9). Since the mass flux and circulation near the centreline are $O(y)$ we conclude from the conservation of mass and circulation that the flow inside this region evolves as a near potential flow with very small azimuthal vorticity, swirl and axial velocity. This situation, together with the boundary condition $\psi_x(x_0, y, t) = 0$, results in an axial velocity in the pipe that is always positive, with no reversed component, specifically, at the outlet $x = x_0$. The flow in the diverging zone evolves uniquely in infinite time into a stagnation zone. The flow inside the stagnation zone comes from an infinitesimal region concentrated around the centreline at the pipe inlet. We want to emphasize that the formation of the stagnation zone in the swirling flow is a natural consequence of the dynamical process described by (1)–(5) and no special assumption has been made to create the stagnation zone. The dynamics of the swirling flow shows that the flow in the stagnation zone is naturally connected with the inlet flow at the centreline. In this way the dynamics of the flow as described by (1)–(5) actually resolves the choice of

the proper continuation model in the analysis of steady and inviscid swirling flows. The results of our numerical simulations using the unsteady Euler equations (1)–(5) (see Rusak *et al.* 1996 and figure 9) confirm this idea and demonstrate that in relevant cases the stagnation model is the proper model to use in the inviscid and steady-state analysis of swirling flows. Actually, we do not use any extra information in addition to the inlet conditions and in this way the stagnation model is not a continuation model.

5. The critical state of a swirling flow in a finite-length pipe

We consider now a base steady swirling columnar flow where $\psi(x, y) = \psi_0(y)$, which is a solution of the SLE (6) and (7). A small-disturbance analysis of the SLE using

$$\psi(x, y) = \psi_0(y) + \epsilon\psi_1(x, y) + ..., \tag{41}$$

where $\epsilon \ll 1$ and ψ_1 is the disturbance stream function, results in the linearized SLE

$$\left.\begin{array}{l} \psi_{1yy} + \dfrac{\psi_{1xx}}{2y} - \left(H''(\psi_0; \omega) - \omega^2\dfrac{\tilde{I}''(\psi_0)}{2y}\right)\psi_1 = 0, \\ \psi_1(x, 0) = \psi_1(x, 1/2) = 0 \text{ for } 0 \leqslant x \leqslant x_0, \\ \psi_1(0, y) = \psi_{1x}(x_0, y) = 0 \text{ for } 0 \leqslant y \leqslant 1/2. \end{array}\right\} \tag{42}$$

Here, $\tilde{I} = K_0^2(y)/2$. This is an eigenvalue problem that has non-trivial solutions only at specific values of ω. This eigenvalue problem was first studied by Squire (1960) and Benjamin (1962) for an infinitely long pipe. Benjamin (1962) defined the first eigenvalue of (42) when x_0 tends to infinity as the critical state, where $\omega = \omega_B$.

We modify Benjamin's critical state concept to the case of a finite-length pipe to reflect the effect of geometry. The 'critical swirl of a flow in a finite length pipe' is defined as the first eigenvalue of (42) and is denoted as ω_1. The critical swirl ω_1 is a bifurcation point of branches of solutions of the SLE where $\psi_1(x, y)$ is given by

$$\psi_1(x, y) = \Phi(y)\sin\left(\dfrac{\pi}{2x_0}x\right) \tag{43}$$

and where ω_1 and Φ are determined by the eigenvalue problem

$$\left.\begin{array}{l} \Phi_{yy} - \left(\dfrac{\pi^2/4x_0^2}{2y} + H''(\psi_0; \omega_1) - \dfrac{\omega_1^2\tilde{I}''(\psi_0)}{2y}\right)\Phi = 0, \\ \Phi(0) = 0, \quad \Phi(1/2) = 0. \end{array}\right\} \tag{44}$$

Notice that as x_0 tends to infinity ω_1 tends to the critical swirl ω_B of Benjamin (1962); ω_1 may also be identified as the transcritical bifurcation point of first sinusoidal solution branch described by Leibovich & Kribus (1990). Using a weakly nonlinear analysis in the case of an infinitely long pipe, Leibovich & Kribus (1990) showed that when $\omega < \omega_1$ the branch of solutions bifurcating at the critical state may describe a solitary wave in the flow.

It is important to point out that from the perspective of variational methods it can be shown (see, for example, Courant & Hilbert 1953) that the columnar flow solution $\psi(x, y) = \psi_0(y)$ is a local minimizer of the functional $\mathscr{E}(\psi)$ when $\omega < \omega_1$. Moreover, at $\omega = \omega_1$ this columnar solution is an inflection point of $\mathscr{E}(\psi)$ where the first and second variations of $\mathscr{E}(\psi)$ vanish. This is similar to the behaviour of the columnar functional $E(\psi)$ at ω_B (see figure 4*f*). We will use these results in the next section to
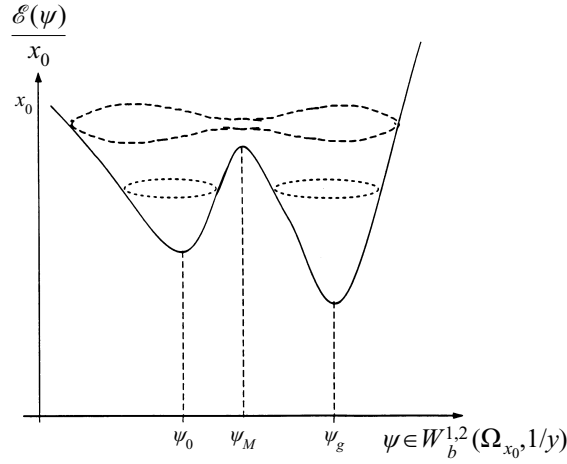
FIGURE 11. The functional $\mathscr{E}(\psi)/x_0$ for $\omega_0 < \omega < \omega_1$.

show the existence of a min-max solution of the SLE (6) for every ω in the range $\omega_0 < \omega < \omega_1$.

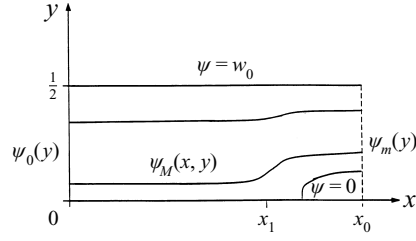## 6. Min-max solution of SLE when $\omega_0 < \omega < \omega_1$

In the previous sections we found that when $\omega > \omega_0$ the global minimizer $\psi_g(x, y)$ of $\mathscr{E}(\psi)$ is very different from the columnar flow $\psi_0(y)$ that is the global minimizer of $\mathscr{E}(\psi)$ when $\omega \leqslant \omega_0$. Also, from the discussion in the end of §5, we find that the columnar flow $\psi(x, y) = \psi_0(y)$ is a local minimizer of $\mathscr{E}(\psi)$ when $\omega_0 < \omega < \omega_1$. Therefore, for each ω in the range $\omega_0 < \omega < \omega_1$ there exist two minimizer solutions of $\mathscr{E}(\psi)$. Consequently, if the functional $\mathscr{E}(\psi)$ is well behaved, one may expect for any ω in the range $\omega_0 < \omega < \omega_1$ the existence of another, third, stationary point of $\mathscr{E}(\psi)$, between the local minimizer $\psi_0(y)$ and the global minimizer $\psi_g(x, y)$, that is a min-max point of $\mathscr{E}(\psi)$ (see figure 11).

We rigorously prove in Appendix C (Theorem C.1) the existence of a min-max solution $\psi_M(x, y)$ of the SLE (6) for any swirl $\omega_0 < \omega < \omega_1$. The proof uses the 'Mountain-Pass Theorem' from nonlinear analysis. The existence of the min-max solution is strongly related to the drastic change in nature of the global minimizer solution as ω changes around ω_0 and the co-existence of two minimizers when $\omega_0 < \omega < \omega_1$. The branch of the min-max solutions bifurcates from the critical state at $\omega = \omega_1$ and is connected to the branch of global minimizer solutions when ω is close to ω_0^+.

In Appendix D we study the properties of the min-max solution $\psi_M(x, y)$. We show that the min-max solution describes a swirling flow in a pipe that may have a localized stagnation zone near the outlet (see figure 12). Along most of the pipe the min-max solution $\psi_M(x, y)$ describes a near columnar flow that is deflected in the radial direction only near the outlet.

We now study the min-max solution $\psi_M(x, y)$ when $\omega < \omega_1$ but ω is close to ω_1. When $\omega = \omega_1$, the columnar solution $\psi(x, y) = \psi_0(y)$ is an inflection point of $\mathscr{E}(\psi)$. Using asymptotic analysis as described in Leibovich & Kribus (1990) (see also Wang & Rusak 1996b) it can be shown that as ω tends to ω_1 there exists a branch of

FIGURE 12. The min-max solution $\psi_M(x, y)$ when $\omega_0 < \omega < \omega_1$.

solutions described by the asymptotic formula

$$\psi(x, y; \omega) = \psi_0(y) + (\omega^2 - \omega_1^2)\kappa_0\psi_1(x, y) + \dots \qquad (45)$$

where $\psi_1(x, y)$ is given by (43) and (44) and

$$\kappa_0 = -2 \frac{\displaystyle\int_0^{1/2}\int_0^{x_0} \frac{\tilde{I}'(\psi_0)}{2y^2\psi_{0y}}\psi_1^2(x, y)\mathrm{d}x\mathrm{d}y}{\displaystyle\int_0^{1/2}\int_0^{x_0}\left(\omega_1^2\frac{\tilde{I}'''(\psi_0)}{2y} - H'''(\psi_0; \omega_1^2)\right)\psi_1^3(x, y)\mathrm{d}x\mathrm{d}y}. \qquad (46)$$

It can be shown that for vortex flows of interest $\kappa_0 < 0$. Calculations of $\mathscr{E}(\psi)$ show that $\mathscr{E}(\psi_0(y)) < \mathscr{E}(\psi(x, y))$ when $\omega < \omega_1$ but close to ω_1 and, therefore, (46) gives an asymptotic expression of the min-max solution as ω tends to ω_1^-. The asymptotic solution (46) describes an almost columnar swirling flow with slightly deflected streamlines in the radial direction.

When $\omega < \omega_1$ but not so close to ω_1 and when the pipe is rather long (when x_0 is of the order of $1/(\omega_1 - \omega)$) Leibovich & Kribus (1990) show that the asymptotic expansion (46) is not valid since nonlinear effects become dominant. Using a multiple-scale weakly nonlinear analysis similar to that given by Leibovich & Kribus (1990) it can be shown that the min-max solution describes a localized (close to solitary) standing wave near the outlet when $\omega < \omega_1$ but not so close to ω_1. When ω is further reduced the localized standing wave grows in size and establishes a local stagnation zone near the outlet (see figure 12 and the discussion in Appendix D).

When ω decreases toward the value ω_0, the branch of min-max solutions $\psi_M(x, y)$ is connected with a special branch of local minimizers of $\mathscr{E}(\psi)$, denoted by $\psi_L(x, y)$, and both bifurcate at about ω_0. The behaviour of solutions of the SLE near ω_0, and specifically the characteristics of the solutions $\psi_L(x, y)$, are complicated and described in detail at the end of Appendix D. It can be shown that the branch of local minimizer solutions $\psi_L(x, y)$ develops naturally and continuously, as ω increases above $\omega_0 + \epsilon(x_0)$, into the branch of global minimizer solutions $\psi_g(x, y)$ describing a vortex breakdown state. Here, ϵ depends on the pipe length x_0 and tends to zero as x_0 tends to infinity.

7. Bifurcation diagram of solutions of the SLE

We can now summarize the global bifurcation diagram of solutions of the SLE as ω changes between 0 and ω_1^+, see figure 13. Each line in figure 13 represents a schematic behaviour of the function $\mathscr{E}(\psi)$ for a fixed level of swirl ω and an extremum represents a solution of the SLE (6) and (7).
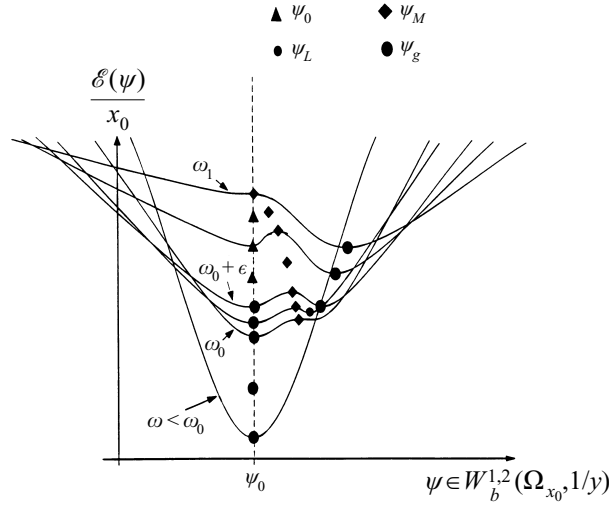
FIGURE 13. The bifurcation diagram of solutions of the SLE.

(*a*) When ω is less than or equal to ω_0 there is only one possible solution of (6) and (7), the columnar flow $\psi_0(y)$ throughout the pipe, which is also the global minimizer of $\mathscr{E}(\psi)$ in this range of ω.

(*b*) When $\omega_0 < \omega \leqslant \omega_0 + \epsilon(x_0)$ there are three possible solutions of (6) and (7): the columnar flow solution $\psi_0(y)$ which is still a global minimizer of $\mathscr{E}(\psi)$, the min-max solution $\psi_M(x,y)$, and the local minimizer solution denoted by $\psi_L(x,y)$. This short branch of local minimizer solutions connects the min-max branch and the global minimizer branch, describing a vortex breakdown state. For a relatively long pipe it is understood that the branch of min-max solutions and the branch of global minimizer solutions are almost connected to each other at about ω_0.

(*c*) When $\omega_0 + \epsilon(x_0) < \omega \leqslant \omega_1$ there are three possible solutions of (6) and (7): the columnar flow solution, $\psi_0(y)$, that is now a local minimizer of $\mathscr{E}(\psi)$, the min-max solution $\psi_M(x,y)$ which describes a localized standing wave in the swirling flow, and the global minimizer solution $\psi_g(x,y)$, which describes a large open stagnation zone in the swirling flow.

(*d*) As the swirl is increased slightly above the critical level, ω_1, the columnar flow solution becomes a min-max point of $\mathscr{E}(\psi)$ and a new branch of local minimizer solutions bifurcates at ω_1 and may describe a non-columnar flow where the rotation rate is increased along the pipe and has a smaller vortical core at the outlet. The third possible solution when $\omega > \omega_1$ is the global minimizer solution described above, where it can now be shown that the stagnation zone becomes much larger and its nose moves toward the inlet.

The results also show that the critical swirl is actually a transcritical bifurcation point from which various branches of local minimizer solutions and min-max solutions may develop.

The bifurcation diagram in figure 13 can now be given in terms of figure 1 that was also used by Beran & Culick (1992) and Buntine & Saffman (1995). Here, again, the minimum axial velocity along the pipe centreline found in each solution is used as a parameter characterizing the solution, see figure 14. We can see that the bifurcation diagram of the SLE (steady-state solutions of Euler equations) is strongly related to the theories of Benjamin (1962), Leibovich & Kribus (1990) and the special solution
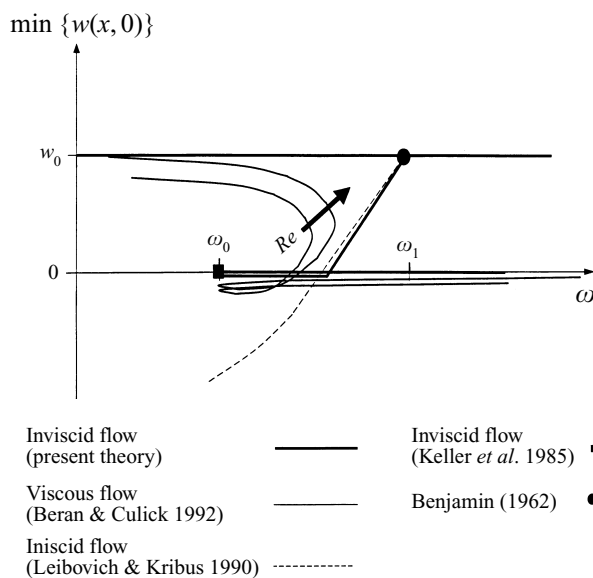
min $\{w(x, 0)\}$

FIGURE 14. The bifurcation diagram of figure 13 given in terms of figure 1.

of Keller *et al.* (1985) and provides the natural relations between the various solutions as well as fills the gap between them. It is also evident that the bifurcation diagram of the SLE correlates nicely with the bifurcation diagram resulting from the numerical simulations of high-Reynolds-number swirling flows using the steady Navier–Stokes equations (see Beran & Culick 1992). Figure 14 suggests that the bifurcation diagram of the steady and viscous solutions is strongly dominated by the steady and inviscid bifurcation diagram when the Reynolds number is sufficiently large. The relations between these diagrams will be discussed in more detail in §10.

In the following section we return to study the dynamics of a swirling flow described by (1)–(5) and, specifically, we discuss the stability of the various branches of steady-state solutions of the SLE. We will show the relation between the critical state at the swirl level ω_1 and the stability of the swirling flow solutions bifurcating at ω_1.

8. Summary of stability analyses

The dynamics of a swirling flow described by (1) with boundary conditions (3) and (4) and initial conditions (5) is strongly related to the bifurcation diagram for the steady-state solutions as given in figures 13 and 14. Of specific interest is the dynamics of swirling flows near the critical state. From the theory of dynamical systems it is strongly expected that the critical level of swirl is also a point of exchange of stability (see Ioos & Joseph 1980).

The linear stability to axisymmetric disturbances of the various branches of solutions bifurcating at the critical state has been recently studied by Wang & Rusak (1996*a*, *b*). A linearized set of equations for the development of infinitesimal axially symmetric disturbances imposed on a base rotating columnar flow has been derived from (1)–(5). Then, a general mode of axisymmetric disturbances, that is not limited to the axial-Fourier mode, has been introduced and an eigenvalue problem was obtained. Asymptotic analyses of the eigenvalue problem near the critical state for both the columnar and non-columnar branches of solutions bifurcating at the critical state
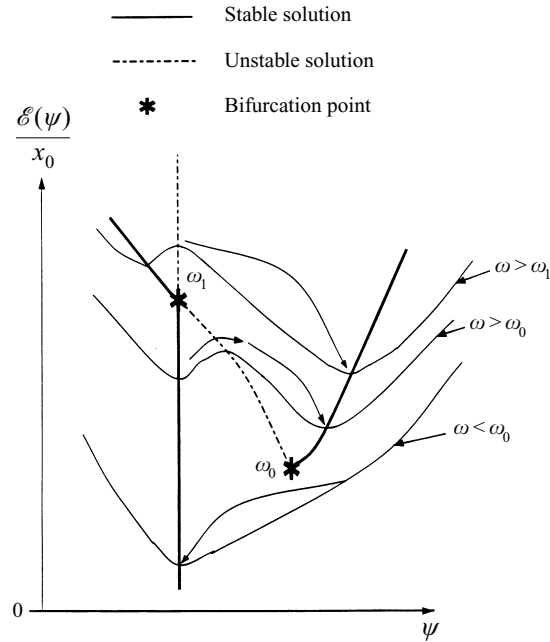
FIGURE 15. The bifurcation diagram and stability characteristics.

have revealed an unknown instability mechanism that cannot be detected by any of the previously known stability analyses. It has been shown that the critical level of swirl is a point of exchange of stability. It has been found that the branches of local minimizer solutions have an asymptotically stable mode of disturbance whereas the branches of min-max solutions are unstable (see figure 15).

The results presented in Wang & Rusak (1996*a*) also provide an interesting physical picture, specifically for the stability of columnar swirling flows. For example, let us consider a uniform axial flow in a straight pipe. When there is no swirl, the flow cannot sustain any disturbance and any initial disturbance is convected downstream by the axial flow and is swept out from the flow domain in a finite time. When swirl is introduced, infinitesimal disturbances to the flow propagate at different speeds that depend on the swirl level (see Benjamin 1962). There exists the critical level of swirl, ω_1, where the maximum speed of the infinitesimal disturbances propagating upstream is equal to the axial speed of the base flow. In this case the flow can sustain a neutrally stable standing small-disturbance wave with a finite length. This mode of disturbance is linearly stable at a supercritical state ($\omega < \omega_1$) because less swirl results in a smaller maximum speed of disturbances propagating upstream and, therefore, the washout effect of the axial flow is more dominant, resulting in the decay of the disturbance in time. However, when the swirl is greater than the critical level ($\omega > \omega_1$), the disturbance mode is unstable since higher swirl results in higher maximum speed of disturbances propagating upstream and, therefore, they become more dominant. Since the inlet conditions (3) for the axial and circumferential velocity components and the azimuthal vorticity are fixed for all time, the small disturbance moving upstream cannot propagate through the incoming flow and, therefore, tends to accumulate and create an instability. This axisymmetric instability mechanism may be observed in Sarpkaya's (1971) experiments and in the recent experiments of Bruecker & Althaus (1995) and Malkiel *et al.* (1996) where the growth of the axisymmetric breakdown

may be associated with an unstable axisymmetric eigen-mode disturbance near the pipe inlet and the upstream propagation of this disturbance.

This inviscid instability mechanism is strongly related to the critical-state concept of Benjamin (1962). However, it should be pointed out that in the case of a swirling flow in an infinitely long pipe, such an exchange of stability around the critical state does not exist since the waves are free to propagate both upstream and downstream and there is no interaction between the waves moving upstream and the inlet conditions. For example, in the case of a solid-body rotating flow with a uniform axial velocity component in an infinitely long pipe Rayleigh's (1916) classical stability criterion predicts that the flow is stable to any axisymmetric disturbance for any swirl level, whereas the analytical solutions presented in Wang & Rusak (1996a) have demonstrated that such a flow in a finite-length pipe changes its stability characteristics as the swirl changes around the critical level of swirl ω_1 of that flow. When $\omega > \omega_1$ the solid-body rotating flow with a uniform axial velocity component is unstable.

9. Mechanism leading to the axisymmetric vortex breakdown in a pipe

The bifurcation diagram and the stability results are now used to explain the development in time of a swirling flow described by (1)–(5). Although not yet rigorously proven, it is strongly expected that the stability results of Wang & Rusak (1996a, b) near the critical state can be extended to the entire branches, i.e. the branches of local and global minimizer solutions are supercritical states (this results from the relevant eigenvalue problem) and asymptotically linearly stable to axisymmetric disturbances. On the other hand, the branches of min-max solutions are unstable (see figure 15). Moreover, the above results may indicate that the branch of columnar flow solutions is unconditionally stable to any axisymmetric disturbance when $\omega < \omega_0$. This means that, for this range of swirl, any axisymmetric disturbance to a base columnar flow will decay in time and the flow will return to a columnar state.

In the range of incoming swirl $\omega_0 < \omega < \omega_1$ two steady-state solutions co-exist: one is a local minimizer solution that describes a columnar swirling flow all along the pipe and the other is a global minimizer solution that describes a swirling flow with a large stagnation zone. Both solutions are stable to small, but finite, axisymmetric disturbances. The two branches of solutions are connected by a branch of min-max solutions that are unstable. This suggests that in the range $\omega_0 < \omega < \omega_1$ there exist two basins of attraction. Which of the two solutions is actually realized depends on the initial disturbances to the base columnar flow. When the initial disturbances are relatively small they will decay in time and the flow will return to a columnar state all along the pipe. However, when the initial disturbances are relatively large they will evolve in time in a complicated nonlinear dynamical process into large disturbances. These will propagate upstream, interact with the inlet state and develop into the vortex breakdown state described by the global minimizer solution.

In the range $\omega > \omega_1$ the equilibrium columnar flow state is unstable and it is expected to be absolutely unstable. Therefore, any axisymmetric disturbance will grow in time through the instability mechanism that depends on the upstream propagation of waves, described in §8. In this range of relatively large incoming swirl it is expected that the global minimizer solution is a strong attractor. Then, the flow again will evolve nonlinearly, with large disturbance waves that propagate upstream and interact with the inlet state. The flow will develop from a columnar state into the vortex breakdown state described by the global minimizer solution.

Our recent numerical simulations based on the time-dependent equations (1)–(5) for a base flow described by the Burgers vortex model (36) fully demonstrate the above results (see Rusak *et al.* 1996). As predicted by this study, we observe the stability of supercritical states and the instability of subcritical states to axisymmetric disturbances. We also observe the unconditional stability of columnar swirling flows when $\omega < \omega_0$, the two basins of attraction in the range $\omega_0 < \omega < \omega_1$ and the strong dependence on initial disturbances in this range of swirl, and the absolute instability of columnar swirling flows when $\omega > \omega_1$. The simulations based on the unsteady and axisymmetric Euler equations also show that in the range $\omega > \omega_0$, the flow always evolves into a steady-state solution and a stagnation zone is always naturally established once the flow evolves into the global minimizer breakdown solution.

The computations in Rusak *et al.* (1996) show that the flow state at ω_1 is a critical state for infinitesimal axisymmetric disturbances (as originally suggested by Benjamin 1962) whereas the flow state at ω_0 is a critical state for large-amplitude disturbances. This means that infinitesimal axisymmetric disturbances can propagate upstream only when $\omega > \omega_1$ whereas large-amplitude disturbances can propagate upstream only when $\omega > \omega_0$. The computations also demonstrate the relation between the upstream propagation of the disturbances in a swirling flow, their interaction with the inlet state and the development of the axisymmetric vortex breakdown.

The above results shed new light on the physical mechanism leading to the axisymmetric vortex breakdown phenomenon in high-Reynolds-number swirling flows in a pipe. As the swirl along the inlet of the pipe is increased toward the critical level ω_1, the base columnar vortex flow tends to lose its stability margin and, definitely, above the critical level, it is unstable. Therefore, when the incoming flow has a swirl level $\omega > \omega_0$, that is near or above the critical swirl ω_1, small axisymmetric disturbances propagate upstream and evolve into large disturbances that interact with the inlet state and become trapped. The flow will dynamically evolve from a columnar state to another axisymmetric equilibrium state that has a separation zone and is described by the global minimizer solution.

10. Effect of small viscosity

The inviscid analysis described above indicates the importance of the critical swirl as a transcritical bifurcation point of steady-state solutions and as a point of exchange of stability. The transcritical bifurcation of the steady-state solutions is a structurally unstable bifurcation, i.e. once small corrections such as small viscous effects are introduced to the steady-state equations the nature of the bifurcation diagram near the critical state may change.

In a recent paper Wang & Rusak (1997) studied the corrections to the inviscid bifurcation diagram due to the existence of small viscosity. Asymptotic techniques were used in the limit where the viscosity tends to zero. Wang & Rusak (1997) demonstrated the singular behaviour of solutions of the Navier–Stokes equations around the critical swirl, ω_1, and provided an explanation of Hall's (1967) boundary layer separation analogy to vortex breakdown. They also showed that the inviscid transcritical bifurcation diagram described in figure 14 indeed breaks into two branches of solutions. Two saddle fold bifurcation points of solutions of the axisymmetric Navier–Stokes equations exist from both sides of the critical swirl, ω_{cv1} and ω_{cv2}, where $\omega_{cv1} = \omega_1 - Cv^{1/2}$ and $\omega_{cv2} = \omega_1 + Cv^{1/2}$. Here C is a constant that can be calculated from the characteristics of the base columnar swirling flow
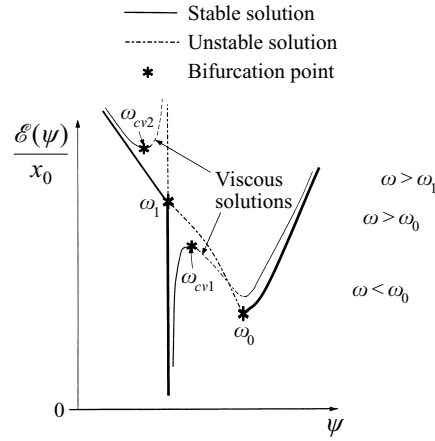
FIGURE 16. The bifurcation diagram and stability characteristics for high-Reynolds-number swirling flows.

(see figure 16). Compared with the inviscid analysis we find that the branch of near columnar flows due to viscosity correction is connected with the branch of min-max solutions with viscosity correction when $\omega < \omega_{cv1}$. The branch of local minimizer solutions with viscosity correction is connected with the branch of near columnar flow solutions with viscosity correction when $\omega > \omega_{cv2}$. It is now clear that the bifurcation diagram obtained by Beran & Culick (1992) matches with only one of the branches resulting from our viscous analysis. Actually, Beran & Culick (1992) searched for the steady-state axisymmetric solutions along a branch that starts from a state with zero swirl. According to our analysis it is clear that there exists one more branch of steady-state axisymmetric solutions of the Navier–Stokes equations when $\omega > \omega_{cv2}$ and that was not found by the continuation method of Beran & Culick (1992).

The recent numerical simulations of Lopez (1994) and Beran (1994) extended the work of Beran & Culick (1992). Based on simulations of swirling flows in a pipe using the unsteady and axisymmetric Navier–Stokes equations they demonstrated that when the Reynolds number is sufficiently large there exist two branches of stable solutions: one that describes an almost columnar flow and another that describes a breakdown solution, and both are part of one branch with a fold, the part of the branch in the fold being unstable. These numerical results show that for high-Reynolds-number flows the stability characteristics of the various branches of solutions of the Navier–Stokes equations are directly inherited from the inviscid mechanism as described in §8.

Moreover, the branch of solutions when $\omega > \omega_{cv2}$, that is missing in the bifurcation diagram of Beran & Culick (1992), may also inherit the stability characteristics of the corresponding inviscid solutions. Therefore, it is expected that the viscosity-corrected columnar swirling flows with $\omega > \omega_{cv2}$ are unstable (see figure 16). We find in this way that the structurally unstable bifurcation of inviscid steady solutions at the critical swirl ω_1 coincides with the exchange of dynamical stability at ω_1. However, the structurally unstable bifurcation will still indicate the existence of a steady near columnar flow solution when the incoming flow is subcritical ($\omega > \omega_1$), specifically when ω is larger than ω_1. Such a steady solution cannot be accessed by a dynamical process since stability analysis indicates that it is linearly unstable.

In this way, it is the dynamical stability characteristics of solutions that play the essential role in explaining the mechanism leading to the vortex breakdown in a pipe and not the structurally unstable bifurcation of inviscid solutions at the critical swirl.

It should be pointed out that the numerical simulations of Lopez (1994) using the axisymmetric time-dependent Navier–Stokes equations also show that for sufficiently large-Reynolds-number swirling flows the separation zones in breakdown solutions are large and essentially stagnant. These are similar in nature to those found in our inviscid computations. We strongly believe that the branch of breakdown solutions described by Beran & Culick (1992) and Lopez (1994) when the Reynolds number is large enough are global minimizer solutions with viscosity correction. Moreover, the size of the separation zones in the viscous computations is comparable to those predicted by our analysis. Based on his numerical simulations Lopez (1994) also suggested that the viscous dissipation is responsible for closing the separation zone and this is not due to the downstream boundary condition. This suggests that in the inviscid limit the bubble will become longer and an open separation zone will appear, as results from our inviscid approach. Furthermore, Lopez (1994) showed that the level of swirl above which breakdown solutions can be found (his secondary limit point) for an inlet Burgers vortex (36) with $\beta = 4.0$ tends to a certain limit value 1.466 as the Reynolds number is increased. Using our method of computing ω_0 (see §3.3 and figure 7) we find that the threshold value for the appearance of inviscid breakdown solutions, in the geometrical scale of Lopez's (1994) computations, is 1.461 which is in good agreement with the viscous computations.

The above discussion suggests that our inviscid approach based on (1)–(5) is the inviscid-limit theory of the axisymmetric and viscous flow problem. When the viscosity is small the present theory describes a dynamical behaviour of axisymmetric swirling flows in a pipe that is close to that computed by Beran & Culick (1992) and Lopez (1994). However, it is expected that when the viscosity is much larger, the viscous effects may change the entire dynamical behaviour. Specifically, ω_{cv1} and ω_0 will coincide, the fold in the bifurcation diagram in figure 16 will be eliminated and only one branch of steady-state solutions will appear. This was actually described by Beran & Culick (1992) and Lopez (1994) for relatively low-Reynolds-number flows. The dynamical behaviour of low-Reynolds-number swirling flows is qualitatively different from the high-Reynolds-number case. The exchange of stability related to the critical swirl is lost when the viscous effects are strong. In such cases the evolution in time from one state to another does not exist and the breakdown zone will appear and grow in size in a continuous process as the incoming swirl is increased. Large-viscosity effects will also result in closing the separation zone after a relatively short distance from the nose of the zone and in the creation of an internal recirculation flow in the zone through the diffusion of momentum from the outer flow into the separation zone.

11. Discussion

We study in this paper the dynamics of inviscid and incompressible axisymmetric swirling flows in a finite-length pipe described by the Euler equations (1) and (2) with the boundary conditions (3) and (4) and the initial conditions (5). This theoretical model may represent a physical situation of a flow in a pipe as is found in some experiments. The analysis is based on studying the flow stability characteristics and

the long-time dynamics of the flow as it is related to steady-state solutions of the problem. Under this framework we provide a theoretical understanding of the dynamics of axisymmetric swirling flows in a pipe.

We summarize the major results found in our analysis. There exist two characteristic swirl levels of the incoming flow to the pipe, ω_0 and ω_1, where $\omega_0 < \omega_1$, and both can be determined by solving ODE problems. Swirling columnar flows with a swirl level less than the threshold level $\omega_0(< \omega_1)$ are unconditionally stable to any axisymmetric disturbance. In the range $\omega_0 < \omega < \omega_1$ we find that, starting from initial disturbances, the flow may evolve into one of two distinct steady states, depending on the size of the initial disturbances. When the disturbances are sufficiently small they will decay in time and the flow will return to a columnar state. However, when the initial disturbances are large enough, they will grow in time and evolve nonlinearly into a large stagnation region in the swirling flow. When $\omega > \omega_1$, the initial disturbances always grow and evolve again into a vortex breakdown solution. Those results clarify the mechanism leading to the axisymmetric vortex breakdown phenomenon in high-Reynolds-number swirling flows. As the incoming swirl level is increased above ω_0, and is near or above ω_1, the columnar swirling flow loses its stability and develops into a breakdown state. This mechanism is governed by the propagation of small- and large-amplitude disturbances in the pipe and its interaction with the inlet conditions.

Our recent numerical computations, guided by the present study, confirm the predicted results and provide details of the nonlinear dynamics of the flow (see Rusak *et al.* 1996). The study also shows good agreement with the numerical computations of Beran & Culick (1992), Beran (1994) and Lopez (1994) using the axisymmetric Navier–Stokes equations when the Reynolds number is sufficiently large. The good agreement suggests that the present approach based on the Euler equations is the inviscid-limit theory of the axisymmetric and viscous flow problem. Our recent experiments guided by the present study (see Malkiel *et al.* 1996) demonstrate the loss of stability of a columnar state and the development in time of the breakdown state. Moreover, the experiments of Malkiel *et al.* (1996) verify the existence of the two limit points of swirl and the existence of two stable and steady states, one of a near columnar flow and the other of a breakdown state, for the same inlet conditions when the swirl level is between the two limit points. The experiments also show the appearance of a breakdown state when the inlet swirl level is above the critical swirl.

This present model explains the suddenness of the vortex breakdown phenomena, specifically around ω_0 where a large disturbance to the basic flow may occur for the first time as the incoming swirl is increased, the abrupt nature of the phenomena due to the development of breakdown zones in the flow, as well as the non-uniqueness of the phenomena in high-Reynolds-number flows, related to the process of increasing the incoming swirl. All of these characteristics are similar to those found in the experiments of Sarpkaya (1971, 1995), Leibovich (1978, 1984) and Bruecker & Althaus (1995) where axisymmetric breakdown zones were found. Also, as demonstrated in figure 14, the present approach connects most of the previously suggested models of vortex breakdown and provides guidelines for future numerical simulations of and experiments on these complicated phenomena.

The present study is limited to inviscid and axisymmetric swirling flows and does not consider the vortex generation mechanism and its interaction with the vortex breakdown phenomenon. Specifically, we would like to point out that the unsteady and axisymmetric problem (1)–(5) has solutions that always evolve into a supercritical

steady-state that is stable to axisymmetric disturbances. However, such steady-state solutions may not necessarily be stable to non-axisymmetric disturbances. If these steady states are unstable to three-dimensional disturbances it is likely that unsteady vortical flows will develop and never settle to a steady state. We believe that in order to study such swirling flows with three-dimensional waves it would appear important to extend our theoretical framework to investigate the development of three-dimensional disturbances from the axisymmetric breakdown solution of our study. These studies might result in more details of the flow dynamics and structure, and the possible evolution of the spiral breakdown out of the axisymmetric breakdown as was found in Bruecker & Althaus's (1995) experiments.

Appendix A. Existence of global minimizer
A.1. *Notation and functional space*

Let $\Omega_{x_0} = (0, x_0) \times (0, 1/2)$ where x_0 is a positive number. Let

$$L^p(\Omega_{x_0}) = \left\{ f : \Omega_{x_0} \to f,\ f \text{ is measurable},\ \int_0^{x_0} \int_0^{1/2} |f|^p \mathrm{d}y \mathrm{d}x < +\infty \right\}$$

with $1 \leqslant p \leqslant \infty$, and

$$\|f\|_{L^p(\Omega_{x_0})} = \left(\int_0^{x_0} \int_0^{1/2} |f|^p \mathrm{d}y \mathrm{d}x \right)^{1/p}.$$

Let

$$W^{1,p}(\Omega_{x_0}) = \left\{ f : f \in L^p(\Omega_{x_0}) \text{ and } \int_0^{x_0} \int_0^{1/2} (|f_y|^p + |f_x|^p) \mathrm{d}y \mathrm{d}x \text{ bounded} \right\}, 1 \leqslant p \leqslant \infty,$$

be the usual Sobolev space with the norm

$$\|f\|_{W^{1,p}(\Omega_{x_0})} = \left(\int_0^{x_0} \int_0^{1/2} (|f|^p + |f_y|^p + |f_x|^p) \mathrm{d}y \mathrm{d}x \right)^{1/p}.$$

Let $W^{1,p}(\Omega_{x_0}, 1/y)$ be the weighted Sobolev space

$$W^{1,p}\left(\Omega_{x_0}, \frac{1}{y}\right) = \left\{ f : f \in L^p(\Omega_{x_0}) \text{ and } \int_0^{x_0} \int_0^{1/2} \left(|f_y|^p + \frac{|f_x|^p}{y} \right) \mathrm{d}y \mathrm{d}x < \infty \right\}, 1 \leqslant p < \infty$$

and

$$\|f\|_{W^{1,p}(\Omega_{x_0}, 1/y)} = \left(\int_0^{x_0} \int_0^{1/2} \left(|f_y|^p + \frac{|f_x|^p}{y} + |f|^p \right) \mathrm{d}y \mathrm{d}x \right)^{1/p}.$$

Set

$$C_b^\infty(\Omega_{x_0}) = \{ f \in C^\infty(\Omega_{x_0}) : f(0, y) = \psi_0(y), f(x, 0) = 0 \text{ and } f(x, 1/2) = w_0 \}$$

and let

$$W_b^{1,p}(\Omega_{x_0}) = \text{ the closure of } C_b^\infty(\Omega_{x_0}) \text{ in } W^{1,p}(\Omega_{x_0})$$

and

$$W_b^{1,p}(\Omega_{x_0}, 1/y) = \text{ the closure of } C_b^\infty(\Omega_{x_0}) \text{ in } W^{1,p}(\Omega_{x_0}, 1/y).$$

A.2. Existence

We seek the following minimizer:

$$\min_{\psi \in W_b^{1,p}(\Omega_{x_0}, 1/y)} \mathscr{E}(\psi). \tag{A1}$$

The global minimizer (A 1), if it exists, denoted by $\psi_g(x, y)$, is a weak solution of (6) and (7), i.e.

$$\int_0^{x_0} \int_0^{1/2} \left(\psi_{gy}\phi_y + \frac{\psi_{gx}\phi_x}{2y} + H'(\psi_g)\phi - \frac{I'(\psi_g)\phi}{2y} \right) \mathrm{d}y\mathrm{d}x = 0 \tag{A2}$$

for all ϕ such that $(\psi_g + \phi) \in W_b^{1,p}(\Omega_{x_0}, 1/y)$. We state the following general existence result:

THEOREM A.1. *Suppose*
1. $H(\psi)$ and $I(\psi)$ are bounded and piecewise smooth non-negative functions with bounded first derivatives;
2. $I(\psi) \leqslant c|\psi|^p$ where p is a fixed number, $1 < p \leqslant 2$, and $c > 0$;
then, the global minimizer of (A 1) *exists.*

The following Hardy's inequality is crucial in our proof of this theorem:

LEMMA A.1. (*Hardy's inequality, see for example Kufner* 1983)
Let $1 < p < \infty$, $u \in C^1[0, x_0]$ with $u(0) = 0$ and

$$\int_0^{x_0} |u'(t)|^p \mathrm{d}t < \infty$$

then, we have

$$\int_0^{x_0} |u(t)|^p t^{-p} \mathrm{d}t \leqslant \left(\frac{p}{p-1} \right)^p \int_0^{x_0} |u'(t)|^p \mathrm{d}t. \tag{A3}$$

Proof of Theorem A.1.   First, we show that the functional $\mathscr{E}(\psi)$ is bounded from below for any $\psi \in W_b^{1,2}(\Omega_{x_0}, 1/y)$. From the boundness of $H(\psi)$, we immediately have

$$0 < \int_0^{x_0} \int_0^{1/2} H(\psi)\mathrm{d}y\mathrm{d}x < m_1. \tag{A4}$$

Let $0 < y_\delta < 1/2$ and for any $\psi \in C_b^\infty(\Omega_{x_0})$, we have

$$\int_0^{x_0} \int_0^{y_\delta} \left| \frac{I(\psi)}{y} \right| \mathrm{d}y\mathrm{d}x \leqslant c \int_0^{x_0} \int_0^{y_\delta} \frac{|\psi|^p}{y} \mathrm{d}y\mathrm{d}x \quad \text{(from assumption 2)}$$

$$\leqslant cy_\delta^{p-1} \int_0^{x_0} \int_0^{y_\delta} \frac{|\psi|^p}{y^p} \mathrm{d}y\mathrm{d}x \quad \text{(since } y \leqslant y_\delta)$$

$$\leqslant cy_\delta^{p-1} \left(\frac{p}{p-1} \right)^p \int_0^{x_0} \int_0^{y_\delta} |\psi_y|^p \mathrm{d}y \quad \text{(Hardy's inequality). (A5)}$$

The above inequality can be extended to the whole space $W_b^{1,2}(\Omega_{x_0})$. From the boundness of $I(\psi)$, we have

$$0 < \int_0^{x_0} \int_{y_\delta}^{1/2} \frac{I(\psi)}{2y} \mathrm{d}y\mathrm{d}x \leqslant m_{y_\delta} \tag{A 6}$$

where m_{y_δ} depends on y_δ.

We now estimate $\mathscr{E}(\psi)$ (equation (8)) as follows:

$$\mathscr{E}(\psi) \geqslant \int_0^{x_0} \int_0^{1/2} \left(\frac{\psi_y^2}{2} + \frac{\psi_x^2}{4y} \right) \mathrm{d}y\mathrm{d}x - \int_0^{x_0} \int_0^{y_\delta} \frac{I(\psi)}{2y} - m_{y_\delta}\mathrm{d}y\mathrm{d}x$$

$$\text{(from (A 4) and (A 6))}$$

$$\geqslant \int_0^{x_0} \int_0^{1/2} \left(\frac{\psi_y^2}{2} + \frac{\psi_x^2}{4y} \right) \mathrm{d}y\mathrm{d}x - c\left(\frac{p}{p-1} \right)^p y_\delta^{p-1} \int_0^{x_0} \int_0^{y_\delta} |\psi_y|^p \mathrm{d}y\mathrm{d}x - m_{y_\delta}$$

$$\text{(from (A 5))}$$

$$\geqslant \frac{1}{4} \int_0^{x_0} \int_0^{1/2} (\psi_y^2 + \psi_x^2)\mathrm{d}y\mathrm{d}x - c\left(\frac{p}{p-1} \right)^p y_\delta^{p-1} |\Omega_{x_0}|^{(2-p)/2} \left(\int_0^{x_0} \int_0^{1/2} \psi_y^2 \mathrm{d}y\mathrm{d}x \right)^{p/2} - m_{y_\delta}$$

$$\text{(from Hölder inequality and where } |\Omega_{x_0}| \text{ is the volume of } \Omega_{x_0} \text{)}$$

$$\geqslant \left(\frac{1}{4} - c_{y_\delta} \right) \int_0^{x_0} \int_0^{1/2} (\psi_y^2 + \psi_x^2)\mathrm{d}y\mathrm{d}x - m_{y_\delta} - c_{y_\delta}$$

$$\text{(from } (\int_0^{x_0} \int_0^{1/2} \psi_y^2 \mathrm{d}y\mathrm{d}x)^{p/2} \leqslant \int_0^{x_0} \int_0^{1/2} \psi_y^2 \mathrm{d}y\mathrm{d}x + 1 \text{ and where}$$

$$c_{y_\delta} = c(p/(p-1))^p y_\delta^{p-1} |\Omega_{x_0}|^{(2-p)/2})$$

$$\geqslant -m_{\tilde{y}_\delta} - c_{\tilde{y}_\delta} = m, \tag{A 7}$$

where we fix $y_\delta = \tilde{y}_\delta$ such that $c_{\tilde{y}_\delta} < \frac{1}{4}$. The boundness of $\mathscr{E}(\psi)$ from below on $W_b^{1,p}(\Omega_{x_0}, 1/y)$ is proven.

From boundness of $H(\psi)$ and $I(\psi)$, $\mathscr{E}(\psi)$ is finite for any $\psi \in W_b^{1,p}(\Omega_{x_0}, 1/y)$ and therefore inf $\mathscr{E}(\psi)$ is finite. Let $\{\psi_i\}$, where $\{\psi_i\} \in W_b^{1,p}(\Omega_{x_0}, 1/y)$ be the minimizing sequence, i.e.

$$\mathscr{E}(\psi_i) \to \inf_{\psi \in W_b^{1,p}(\Omega_{x_0}, 1/y)} \mathscr{E}(\psi).$$

From (A 7),

$$\int_0^{x_0} \int_0^{1/2} \left(\frac{\psi_{iy}^2}{2} + \frac{\psi_{ix}^2}{4y} \right) \mathrm{d}y\mathrm{d}x < \infty,$$

and

$$\int_0^{x_0} \int_0^{1/2} \frac{I(\psi)}{2y} \mathrm{d}y\mathrm{d}x < \infty.$$

By virtue of some variant of the Poincaré inequality (see, for example, Ziemer 1989)

$$\|\psi_i\|_{W_b^{1,2}(\Omega_{x_0}, 1/y)} < \infty.$$

Then, there exists a subsequence of $\{\psi_i\}$, still denoted by $\{\psi_i\}$, such that

$$\psi_i \rightharpoonup \psi_g \text{ weakly in } W_b^{1,2}(\Omega_{x_0}, 1/y), \tag{A 8}$$

and

$$\psi_i \to \psi_g \text{ strongly in } L^p(\Omega_{x_0}), 1 \leqslant p < \infty. \tag{A 9}$$

We claim

$$\mathscr{E}(\psi_g) = \inf_{\psi \in W_b^{1,2}(\Omega_{x_0}, 1/y)} \mathscr{E}(\psi). \tag{A 10}$$

The following inequality is well known (see, for example, Struwe 1990):

$$\varliminf_{i \to \infty} \int_0^{x_0} \int_0^{1/2} \left(\frac{\psi_{iy}^2}{2} + \frac{\psi_{ix}^2}{4y} \right) \mathrm{d}y\mathrm{d}x \geqslant \int_0^{x_0} \int_0^{1/2} \left(\frac{\psi_{gy}^2}{2} + \frac{\psi_{gx}^2}{4y} \right) \mathrm{d}y\mathrm{d}x. \tag{A 11}$$

From (A 9) we have

$$\int_0^{x_0} \int_0^{1/2} H(\psi_i)\mathrm{d}y\mathrm{d}x \to \int_0^{x_0} \int_0^{1/2} H(\psi_g)\mathrm{d}y\mathrm{d}x \quad \text{as } i \to \infty. \tag{A 12}$$

We now estimate the term $\int_0^{x_0} \int_0^{1/2} I(\psi_i)/2y \, \mathrm{d}y\mathrm{d}x$ as follows:

$$\varliminf_{i \to \infty} \left(\int_0^{x_0} \int_0^{1/2} \frac{I(\psi_i)}{2y}\mathrm{d}y\mathrm{d}x - \int_0^{x_0} \int_0^{1/2} \frac{I(\psi_g)}{2y}\mathrm{d}y\mathrm{d}x \right)$$

$$= \varliminf_{i \to \infty} \left(\int_0^{x_0} \int_{y_\delta}^{1/2} \left(\frac{I(\psi_i)}{2y} - \frac{I(\psi_g)}{2y} \right) \mathrm{d}y\mathrm{d}x \right) + \varliminf_{i \to \infty} \int_0^{x_0} \int_0^{y_\delta} \left(\frac{I(\psi_i)}{2y} - \frac{I(\psi_g)}{2y} \right) \mathrm{d}y\mathrm{d}x$$

(here $0 < y_\delta < 1$, and the first limit vanishes from (A 9))

$$= \varliminf_{i \to \infty} \int_0^{x_0} \int_0^{y_\delta} \left(\frac{I(\psi_i)}{2y} - \frac{I(\psi_g)}{2y} \right) \mathrm{d}y\mathrm{d}x$$

$$\leqslant \varliminf_{i \to \infty} \left(c_{y_\delta} \int_0^{x_0} \int_0^{y_\delta} |\psi_{iy}|^2 \mathrm{d}y\mathrm{d}x - \int_0^{x_0} \int_0^{y_\delta} \frac{I(\psi_g)}{2y}\mathrm{d}y\mathrm{d}x \right) \text{ (from (A 7))}$$

$$\leqslant c_{y_\delta} M - \int_0^{x_0} \int_0^{y_\delta} \frac{I(\psi_g)}{2y}\mathrm{d}y\mathrm{d}x \left(\text{from (A 7)}, \int_0^{x_0} \int_0^{1/2} |\psi_{iy}|^2 \mathrm{d}y\mathrm{d}x \text{ is bounded} \right).$$

$$\tag{A 13}$$

Here $M > 0$ is a constant. Combining (A 11), (A 12) and (A 13), we obtain

$$\inf_{\psi \in W_b^{1,2}(\Omega_{x_0}, 1/y)} \mathscr{E}(\psi) = \varliminf_{i \to \infty} \mathscr{E}(\psi_i)$$

$$\geqslant \mathscr{E}(\psi_g) - c_{y_\delta} M + \int_0^{x_0} \int_0^{y_\delta} \frac{I(\psi_g)}{2y}\mathrm{d}y\mathrm{d}x$$

$$\geqslant \mathscr{E}(\psi_g) - c_{y_\delta} M.$$

Let $y_\delta \to 0$, then $c_{y_\delta} M \to 0$ and

$$\inf_{\psi \in W_b^{1,2}(\Omega_{x_0}, 1/y)} \mathscr{E}(\psi) \geqslant \mathscr{E}(\psi_g).$$

However, we must have $\mathscr{E}(\psi_g) \geqslant \inf_{\psi \in W_b^{1,2}(\Omega_{x_0}, 1/y)} \mathscr{E}(\psi)$ and therefore we find that $\mathscr{E}(\psi_g) = \inf_{\psi \in W_b^{1,2}(\Omega_{x_0}, 1/y)} \mathscr{E}(\psi)$. So ψ_g is the global minimizer of $\mathscr{E}(\psi)$. $\qquad\square$

Note the regularity of $\psi_g(x, y)$: $\psi_g(x, y)$ is a weak solution of (6) and (7) as mentioned at the beginning of this section. Let Ω_o be any domain such that $\bar{\Omega}_o \subset \Omega_{x_0}$;

we show that $\psi_g \in C^{2-\delta}(\Omega_o)$ for any $\delta > 0$. Actually, from the boundness and piecewise continuity of $H'(\psi)$ and $I'(\psi)$, we have

$$H'(\psi_g) - \frac{I'(\psi_g)}{2y} \in L^p(\Omega_o), \quad 1 \leqslant p < \infty$$

and by using elliptic regularity theory (see, for example, Gilbarg & Trudinger 1983), we have

$$\psi_g \in W^{2,p}(\Omega_o) \text{ for } 1 \leqslant p < \infty$$

and then

$$\psi_g \in C^{2-2/p}(\Omega_o) \tag{A 14}$$

from the Sobolev embedding $W^{2,p}(\Omega_o, 1/y) \hookrightarrow C^{2-2/p}(\Omega_o)$ (see, for example, Adams 1975). Thus, derivatives of ψ_g are everywhere continuous functions on Ω_{x_0} whether $H'(\psi)$ and $I'(\psi)$ are continuous or not. From the Hölder estimate, at any regular point of $H'(\psi)$ and $I'(\psi)$ we find that $\psi_g(x, y)$ is twice differentiable and is a regular solution of (6) and (7).

Appendix B. Properties of global minimizer

Let

$$W^{1,2}(0, 1/2) = \left\{ \psi \in L^2((0, 1/2)) : \int_0^{1/2} \psi_y^2 \mathrm{d}y \quad \text{is bounded} \right\}$$

with the norm

$$\|\psi\|_{W^{1,2}(0,1/2)} = \left(\int_0^{1/2} (\psi^2 + \psi_y^2) \mathrm{d}y \right)^{1/2}.$$

Also, let

$$C_b^\infty(0, 1/2) = \{ \psi \in C^\infty(0, 1/2) : \psi(0) = 0, \psi(1/2) = w_0 \}$$

and

$$W_b^{1,2}(0, 1/2) = \text{ the closure of } C_b^\infty(0, 1/2) \text{ in } W^{1,2}(0, 1/2).$$

We consider the following eigenvalue problem:

$$\left. \begin{array}{r} \psi_{yy} - \left(H''(\tilde{\psi}) - \dfrac{I''(\tilde{\psi})}{2y} \right) \psi + \lambda \psi = 0, \\ \psi(0) = \psi(1/2) = 0, \end{array} \right\} \tag{B 1}$$

which is related to the linearized SLE in the columnar case. It is a well known fact (see, for example, Courant & Hilbert 1953) that when the smallest eigenvalue of this eigenvalue problem is positive then the following estimate of $E(\psi)$:

$$E(\tilde{\psi} + \psi) - E(\tilde{\psi}) \geqslant C \|\psi\|_{W_b^{1,2}(0,1/2)}^2 \tag{B 2}$$

with $C > 0$, holds for every ψ with $\|\psi\|_{W_b^{1,2}(0,1/2)} < \delta$, where δ is a positive number. Equation (B 2) shows that when the smallest eigenvalue of the problem (B 1) is positive $\tilde{\psi}$ is a strict minimizer of $E(\psi)$. It is important to notice that for vortex flows of interest such as the Rankine vortex model (given by (18) and (19)) and the Burgers

vortex model (given by (34) and (35)) equation (B 2) always holds for the global minimizer solution of the columnar problem.

THEOREM B.1. *Suppose $\psi_s(y)$ is a strictly local minimizer of $E(\psi)$ and the estimate given by* (B 2) *holds around $\psi_s(y)$. Let G_ϵ with $\epsilon > 0$ be the set*

$$G_\epsilon = \{x \in (0, x_0) : \|\psi(x, y) - \psi_s(y)\|_{C^{1/2}(0,1/2)} > \epsilon\} \tag{B 3}$$

then, we have the following estimate of 'length' of G_ϵ

$$m(G_\epsilon) < L_\epsilon \tag{B 4}$$

where L_ϵ does not depend on x_0, the length of the pipe, and $m(G_\epsilon)$ denotes the measure of G_ϵ.

Here $C^{1/2}(0, 1/2)$ is the Hölder space with the norm

$$\sup_{y_1,y_2 \in (0,1/2), y_1 \neq y_2} \frac{|\psi(y_1) - \psi(y_2)|}{|y_1 - y_2|^{1/2}}.$$

Proof. Let $\psi_c(x, y)$ be the comparison function

$$\psi_c(x, y) = \begin{cases} \psi_0(y)(1 - x) + x\psi_s(y) & \text{when } 0 \leqslant x \leqslant 1, \\ \psi_s(y) & \text{when } 1 \leqslant x \leqslant x_0. \end{cases}$$

Here, $\psi_0(y)$ is the inlet flow and ψ_s is the columnar minimizer of $E(\psi)$. Obviously, $\psi_c \in W_b^{1,2}(\Omega_{x_0}, 1/y)$ and

$$\mathscr{E}(\psi_c) = c + (x_0 - 1)E(\psi_s) \tag{B 5}$$

where

$$c = \int_0^1 \int_0^{1/2} \left(\frac{\psi_{cy}^2}{2} + \frac{\psi_{cx}^2}{4y} + H(\psi_c) - \frac{I(\psi_c)}{2y} \right) \mathrm{d}y\mathrm{d}x$$

and we always have $c \geqslant E(\psi_s) > 0$.

For the global minimizer ψ_g of $\mathscr{E}(\psi)$, we have from the definitions of ψ_g and ψ_c

$$\mathscr{E}(\psi_c) \geqslant \mathscr{E}(\psi_g) \geqslant x_0 E(\psi_s). \tag{B 6}$$

Combining (B 5) and (B 6), we obtain the following:

$$\mathscr{E}(\psi_g) - x_0 E(\psi_s) \leqslant c - E(\psi_s). \tag{B 7}$$

From the definition of $\mathscr{E}(\psi)$, we find

$$\frac{\mathscr{E}(\psi_g)}{x_0} \geqslant \frac{1}{x_0} \int_0^{x_0} \int_0^{1/2} \left(\frac{\psi_{gy}^2}{2} + H(\psi_g) - \frac{I(\psi_g)}{2y} \right) \mathrm{d}y\mathrm{d}x$$

and from (B 7), we obtain

$$\int_0^{x_0} \int_0^{1/2} \left(\frac{\psi_{gy}^2}{2} + H(\psi_g) - \frac{I(\psi_g)}{2y} \right) \mathrm{d}y\mathrm{d}x - x_0 E(\psi_s) \leqslant c - E(\psi_s). \tag{B 8}$$

Let $K(x)$ be the function

$K(x) = E(\psi_g(x, y))$, where x is fixed as we calculate $E(\psi_g(x, y))$ according to (11),

and T_δ, with $\delta > 0$, be the set

$$T_\delta = \{x \in (0, a) : K(x) - E(\psi_s) > \delta\}. \tag{B 9}$$

From (B 8), we have

$$\delta \, m \, (T_\delta) \leqslant \int_{T_\delta} (K(x) - E(\psi_s)) \mathrm{d}x \leqslant \int_0^{x_0} (K(x) - E(\psi_s)) \mathrm{d}x \leqslant c - E(\psi_s). \quad \text{(B 10)}$$

Then,

$$m \, (T_\delta) \leqslant \frac{c - E(\psi_s)}{\delta}. \quad \text{(B 11)}$$

From the estimate (B 11) and Sobolev embedding $W_b^{1,2}(0, 1/2) \hookrightarrow C^{1/2}(0, 1/2)$, for any given $\epsilon > 0$, we may find a $\delta(\epsilon)$, that depends on ϵ, such that

$$G_\epsilon \subset T_\delta$$

and, therefore,

$$m \, (G_\epsilon) \leqslant \frac{c - E(\psi_s)}{\delta(\epsilon)}.$$

If $L_\epsilon = (c - E(\psi_s))/\delta(\epsilon)$, we obtain (B 4) and the theorem is proven. $\qquad \square$

Comment: The proof of Theorem B.1 is general for any inlet flow $\psi_0(y)$ and is not limited to the assumption that inlet flow is described by the Rankine or Burgers vortex models.

Appendix C. Existence of min-max solution

We consider the case where $\omega_0 < \omega \leqslant \omega_1$. We shall show that there exists a third solution of the SLE which is not a minimizer (global or local) of $\mathscr{E}(\psi)$. Therefore, a traditional variational approach would not work in the search of this type of stationary point. New methods from non-traditional variational calculus and global analysis are needed. The following theorem known as the 'Mountain Pass theorem' is our main tool in the proof of existence of the third solution of (6) and (7).

THEOREM C.1. (*The Mountain Pass Theorem*) (*see, for example, Struwe* 1990)
Let V be a Banach space and suppose that the functional $F(v)$ is defined on V, $F(v) \in C^1(V)$ and satisfies
(a) there exist $\gamma > 0, \alpha > 0$ and $v_0 \in V$ such that

$$||v - v_0|| = \gamma \Rightarrow F(v) \geqslant \alpha + F(v_0); \quad \text{(C 1)}$$

(b) there exists $v_1 \in V$ where $||v_1|| > \gamma$ and

$$F(v_1) < \alpha + F(v_0); \quad \text{(C 2)}$$

(c) the Palais–Smale condition, i.e. for any sequence $\{v_i\}$ with

$$F'(v_i) \to 0 \text{ in } V' \text{ (dual space of } V)$$

and

$$|F(v_i)| \text{ is bounded}$$

there exists a subsequence of $\{v_{i_k}\}$ such that

$$v_{i_k} \to v_0 \text{ in } V \text{ strongly.}$$

Define the set of path P as

$$P = \{p_{ath} \in C^0([0, 1], V) : p_{ath}(0) = v_0 \text{ and } p_{ath}(1) = v_1\} \quad \text{(C 3)}$$

then

$$\beta = \inf_{p_{ath} \in P} \sup_{t \in [0,1]} F(p_{ath}(t)) \tag{C4}$$

is a stationary value of $F(v)$.

In our case, we may take $W_b^{1,2}(\Omega_{x_0}, 1/y)$ as V and $\mathscr{E}(\psi) = F(v)$. $W_b^{1,2}(\Omega_{x_0}, 1/y)$ is a closed affine subspace of the Hilbert space $W^{1,2}(\Omega_{x_0}, 1/y)$ (and therefore a Banach space) and $\mathscr{E}(\psi) \in C^1(W_b^{1,2}(\Omega_{x_0}, 1/y))$. We can verify the Palais–Smale condition for $\mathscr{E}(\psi)$ by using Hardy's inequality and Rellich–Kondrachov compactness theorem (see, for example, Adams 1975). Therefore, in order to apply the Mountain pass theorem to $\mathscr{E}(\psi)$, we need to verify that the assumptions (*a*) and (*b*) in the Theorem are also satisfied.

THEOREM C.2. *When $\omega_0 < \omega < \omega_1$, and the length of the pipe is sufficiently large, there exist a solution $\psi_M(x, y)$ of (6) and (7) which is obtained by the mountain pass theorem and has a stationary value of $\mathscr{E}(\psi)$ determined by (C 4).*

Proof. Let $p_{ath}(0) = \psi_0(y)$ and $p_{ath}(1) = \psi_g$.

Verification of assumption (*a*). The local behaviour of $\mathscr{E}(\psi)$ near the solution $\psi_0(y)$ is determined by the eigenvalue problem: find ϕ such that

$$\phi_{yy} + \frac{\phi_{xx}}{2y} - \left(H''(\psi_0) - \frac{I''(\psi_0)}{2y}\right)\phi + \lambda\phi = 0 \quad \text{where} \quad \psi_0 + \phi \in W_b^{1,2}(\Omega_{x_0}, 1/y). \tag{C5}$$

The above eigenvalue problem is an extension of (B 1) and when the smallest eigenvalue of (C 5) is positive, an estimate similar to (B 1) can be obtained:

$$\mathscr{E}(\psi_0 + \psi) - \mathscr{E}(\psi_0) \geqslant c\|\psi\|^2_{W_b^{1,2}(\Omega_{x_0}, 1/y)} \text{ for } \|\psi\|_{W_b^{1,2}(\Omega_{x_0}, 1/y)} \leqslant \delta \tag{C6}$$

where $\delta > 0$ is a constant. Let $\gamma = \delta$ and $\alpha = c\delta^2$ we obtain assumption (*a*) from (C 6).

From the definition of the critical swirl ω_1 (see §5) it is clear that when $\omega < \omega_1$, the smallest eigenvalue of (C 5) is always positive.

Verification of assumption (*b*). We have the following estimate from Theorem C.1

$$\frac{\mathscr{E}(\psi_g)}{x_0} \sim E(\psi_s) \quad \text{for large } x_0. \tag{C7}$$

Then,

$$\frac{\mathscr{E}(\psi_0)}{x_0} = E(\psi_0) > E(\psi_s) \sim \frac{\mathscr{E}(\psi_g)}{x_0} \tag{C8}$$

where $\psi_s(y)$ is the global minimizer of the columnar functional $E(\psi)$ and (*b*) follows from (C 8) and assumption (*a*).

We have verified all the conditions in the mountain pass theorem. Therefore, there exists a third solution of (6) and (7) denoted as $\psi_M(x, y)$, which is a min-max point of $\mathscr{E}(\psi)$ and is characterized by (C 4). Figure 11 illustrates the existence of the min-max solution ψ_M between the minimizer solutions ψ_0 and ψ_g. We see that there exists a path from ψ_0 and ψ_g where at the top of the path, we find the solution ψ_M. $\qquad\square$

Appendix D. Properties of the min-max solution $\psi_M(x, y)$

The solution $\psi_M(x, y)$ is obtained in a rather abstract frame. We need to discuss this solution in more detail. We first show the following basic estimate

THEOREM D.1.

$$\frac{\mathscr{E}(\psi_M)}{\mathscr{E}(\psi_0)} \to 1 \text{ as } x_0 \to \infty, \tag{D 1}$$

where x_0 is the length of the pipe.

Proof. Let $\psi_{M_{x_{01}}}$ be the mountain pass solution for $\Omega_{x_{01}}$ where x_{01} is a pipe length that is different from x_0. Let $p_{ath}(t)$ be a path which satisfies

$$\mathscr{E}(\psi_{M_{x_{01}}}) \leqslant \max_{t \in [0,1]} \mathscr{E}(p_{ath}(t)) < \mathscr{E}(\psi_{M_{x_{01}}}) + \epsilon. \tag{D 2}$$

According to Theorem C.1, such a path always exists when $\omega_0 < \omega < \omega_1$. Now, for $\Omega_{x_{01}}$ with $x_0 > x_{01}$, we construct the following path:

$$\tilde{p}_{ath}(t) = \begin{cases} \psi_0 & \text{when } 0 < x < x_0 - x_{01}, \\ p_{ath}(t)(x - (x_0 - x_{01})), y) & \text{when } x_0 - x_{01} \leqslant x \leqslant x_0. \end{cases} \tag{D 3}$$

Notice that when $x_0 - x_{01} \leqslant x \leqslant x_0$, $0 \leqslant x - (x_0 - x_{01}) \leqslant x_0$ thus $p_{ath}(t)(x - (x_0 - x_{01}), y)$ is well defined. Clearly, $\tilde{p}_{ath}(0) = \psi_0$ on Ω_{x_0} and $\mathscr{E}(\tilde{p}_{ath}(0)) \leqslant \mathscr{E}(\tilde{p}_{ath}(1))$ from the fact that $\mathscr{E}(p_{ath}(1)) \leqslant \mathscr{E}(p_{ath}(0))$. Therefore, $\tilde{p}_{ath}(t)$ is an eligible path. Denote $\psi_{M_{x_0}}$ as the mountain pass solution for Ω_{x_0}. Then, from (D 2) we find

$$\mathscr{E}(\psi_{M_{x_0}}) \leqslant \max_{t \in [0,1]} \mathscr{E}(\tilde{p}_{ath}(t)) = (x_0 - x_{01})E(\psi_0) + \max_{t \in [0,1]} \mathscr{E}(p_{ath}(t))$$

$$\leqslant (x_0 - x_{01})E(\psi_0) + \mathscr{E}(\psi_{M_{x_{01}}}) + \epsilon. \tag{D 4}$$

Dividing (D 4) by $\mathscr{E}(\psi_0)$, we have

$$\frac{\mathscr{E}(\psi_{M_{x_0}})}{\mathscr{E}(\psi_0)} = \frac{\mathscr{E}(\psi_{M_{x_0}})}{x_0 E(\psi_0)} \leqslant \left(1 - \frac{x_{01}}{x_0}\right) + \frac{\mathscr{E}(\psi_{M_{x_{01}}})}{x_0 E(\psi_0)} + \epsilon.$$

Now let $x_0 \to \infty$, we get $\mathscr{E}(\psi_{M_{x_0}})/\mathscr{E}(\psi_0) \leqslant 1$. However, since $\mathscr{E}(\psi_0) < \mathscr{E}(\psi_{M_{x_0}})$, we obtain (D 1). □

We now compare the behaviour of the min-max solution $\psi_M(x, y)$ with that of the global minimizer solution $\psi_g(x, y)$. As we have seen in Theorem B 1, we can estimate $\mathscr{E}(\psi_g)/x_0 \sim E(\psi_s)$ as x_0 tends to infinity. From this estimate we can demonstrate that the solution $\psi_g(x, y)$ is dominated, except for a finite transition region near the pipe inlet, by a long region where the flow is close to the columnar state $\psi_s(y)$ (see figure 8). However, the estimate in Theorem D 1 that $\mathscr{E}(\psi_M)/x_0 \sim E(\psi_0)$ as x_0 tends to infinity, shows that the min-max solution is dominated by a long region, starting from the inlet, where the flow is close to the columnar state $\psi_0(y)$ (see figure 12). From the inlet condition $\psi_M(0, y) = \psi_0(y)$ we find that $\psi_{Mx}(0, y)$ is small and when $x_0 \to \infty$ it vanishes. Therefore, a columnar state is established at the inlet when $x_0 \to \infty$.

Let $\psi_m = \psi_M(x_0, y)$. Then, from the flow force balance (15) we find that as the pipe length becomes larger, $E(\psi_0) - \int_0^{1/2} (\psi_{Mx}^2(0, y)/4y)\mathrm{d}y = E(\psi_m(y))$. Thus, $E(\psi_m(y))$ is slightly less than $E(\psi_0)$ and so $\psi_m(y)$ is not close to a columnar solution of (9) and (10), except when ω tends to ω_0, where $\psi_m(y)$ tends to $\psi_K(y)$.

We now describe the min-max solution $\psi_M(x, y)$ of (6) and (7) (see figure 12). At
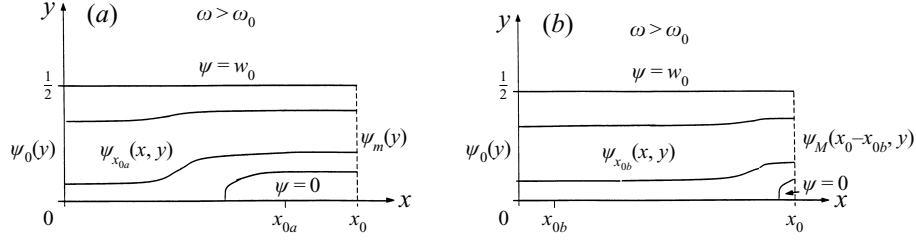
FIGURE 17. The comparison functions (a) $\psi_{x_{0a}}(x, y)$, (b) $\psi_{x_{0b}}(x, y)$.
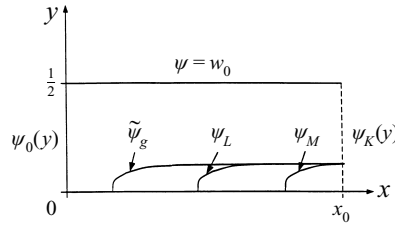
FIGURE 18. The solution ψ_L, ψ_M and $\tilde{\psi}_g$ when $\omega \sim \omega_0$.

the inlet $\psi_M(0, y) = \psi_0$. There exists x_1 where for $0 \leqslant x < x_1$, ψ_M is close to ψ_0. For $x_1 \leqslant x < x_0$, a transition stage from ψ_0 to ψ_m is established.

Let us demonstrate that the solution $\psi_M(x, y)$ described above and in figure 12 is the min-max solution. We choose two families of comparison functions $\psi_{x_{0a}}$ and $\psi_{x_{0b}}$.

(i) The function $\psi_{x_{0a}}$ is given by

$$\psi_{x_{0a}}(x, y) = \begin{cases} \psi_M(x + x_0 - x_{0a}, y), & 0 \leqslant x \leqslant x_{0a}, \\ \psi_m(y) & x_{0a} \leqslant x \leqslant x_0, \end{cases} \quad (D\,5)$$

where $x_{0a} < x_0$ is given, see figure 17(a). Since for any $0 \leqslant x \leqslant x_0$, $E(\psi_m) \leqslant E(\psi_M(x, y))$ with x fixed, we find that $\mathscr{E}(\psi_M) \geqslant \mathscr{E}(\psi_{x_{0a}})$. Now, in the region $x_{0a} \leqslant x \leqslant x_0$ the columnar flow $\psi_{x_{0a}}(x, y) = \psi_m(y)$ is neither a solution of the columnar equation (6) nor the minimizer ψ_s of $E(\psi)$. Thus, a path $p_{ath}(t)$ can be formed, with $p_{ath}(0) = \psi_{x_{0a}}(x, y)$, such that we can push $\mathscr{E}(\psi)$ from $\mathscr{E}(p_{ath}(0))$ toward the global minimizer $\psi_g(x, y)$ of $\mathscr{E}(\psi)$.

(ii) The function $\psi_{x_{0b}}(x, y)$ is given by

$$\psi_{x_{0b}}(x, y) = \begin{cases} \psi_0(y) & 0 \leqslant x \leqslant x_{0b}, \\ \psi_g(x - x_{0b}, y) & x_{0b} \leqslant x \leqslant x_0, \end{cases} \quad (D\,6)$$

where x_{0b} is given, see figure 17(b). As x_{0b} increases $\psi_{x_{0b}}(x, y) \to \psi_0(y)$ everywhere in Ω_{x_0}. This is a path from $\psi_M(x, y)$ to ψ_0 and along this path $\mathscr{E}(\psi_{x_{0b}})$ decreases since for any x_{0b} we find $E(\psi_{x_{0b}}(x_0, y)) \geqslant E(\psi_0)$.

In summary, we find that, $\psi_M(x, y)$ is a local maximum of $\mathscr{E}(\psi)$ along a special direction. This is the feature of the min-max solution.

We now discuss the connection between the branch of min-max solutions $\psi_M(x, y)$ and the branch of the global minimizer solutions $\psi_g(x, y)$ when ω is close to ω_0. First we again notice that for a finite-length pipe, ψ_0 is the global minimizer of $\mathscr{E}(\psi)$ up to $\omega_0 + \epsilon$ with $\epsilon > 0$ and $\epsilon \to 0$ as the length x_0 of the pipe tends to ∞. At $\omega = \omega_0$, any transition along the pipe occurring in the base vortex will result in an increase in
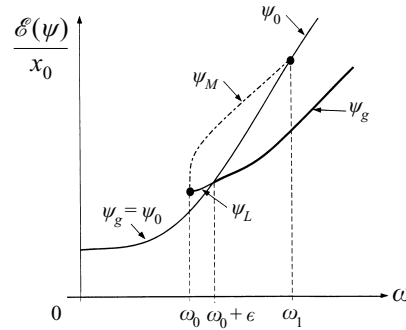
FIGURE 19. The bifurcation diagram of solutions of the SLE.

the value of $\mathscr{E}(\psi)$. Therefore, ψ_0 is the global minimizer of $\mathscr{E}(\psi)$ also at $\omega = \omega_0$. At $\omega = \omega_0 + \epsilon$, the global minimizer switches from ψ_0 to $\tilde{\psi}_g(x, y)$ which is the starting point for the branch of solutions of (6) and (7) that are global minimizers of $\mathscr{E}(\psi)$ when $\omega > \omega_0 + \epsilon$. The solution $\tilde{\psi}_g$ is shown in figure 18. When ω is slightly decreased from $\omega_0 + \epsilon$ a branch of solutions $\psi_L(x, y)$ of (6) and (7) that are local minimizers of $\mathscr{E}(\psi)$ is obtained. This branch of solutions connects the global minimizer solution $\tilde{\psi}_g(x, y)$ at $\omega_0 + \epsilon$ with the branch of min-max solution $\psi_M(x, y)$ (see figure 19).

In order to better understand the branch of solutions $\psi_L(x, y)$, we compare the solutions $\tilde{\psi}_g(x, y)$ at $\omega_0 + \epsilon$, $\psi_L(x, y)$ and $\psi_M(x, y)$, see figure 18. In all of these solutions the outlet flow is close to $\psi_K(y)$ and, therefore, they all describe a similar transition stage from ψ_0 to ψ_K. As ω decreases from $\omega_0 + \epsilon$ the local minimizer $\psi_L(x, y)$ of $\mathscr{E}(\psi)$ describes an intermediate state between $\tilde{\psi}_g(x, y)$ and $\psi_M(x, y)$ where the nose of the stagnation zone moves downstream. Notice that the position of the zone nose is very sensitive to very small changes of swirl ω slightly above ω_0. This special behaviour is also found in our recent computations (see Rusak *et al.* 1997).

REFERENCES

ADAMS, R. A. 1975 *Sobolev Space*. Academic Press.

BATCHELOR, G. K. 1967 *An Introduction to Fluid Dynamics*, pp. 543–555. Cambridge University Press.

BENJAMIN, T. B. 1962 Theory of the vortex breakdown phenomenon. *J. Fluid Mech.* **14**, 593–629.

BERAN, P. S. 1994 The time-asymptotic behavior of vortex breakdown in tubes. *Computers Fluids* **23**, 913–937.

BERAN, P. S. & CULICK, F. E. C. 1992 The role of non-uniqueness in the development of vortex breakdown in tubes. *J. Fluid Mech.* **242**, 491–527.

BRAGG, S. L. & HAWTHORNE, W. R. 1950 Some exact solutions of the flow through annular cascade actuator discs. *J. Aero. Sci.* **17**, 243–249.

BRUECKER, CH. & ALTHAUS, W. 1995 Study of vortex breakdown by particle tracking velocimetry (PTV), Part 3: time-dependent structure and development of breakdown modes. *Exps. Fluids* **18**, 174–186.

BUNTINE, J. D. & SAFFMAN, P. G. 1995 Inviscid swirling flows and vortex breakdown. *Proc. R. Soc. Lond.* A **449**, 139–153.

COURANT, R. & HILBERT, D. 1953 *Methods of Mathematical Physics*. Interscience.

DARMOFAL, D. L. 1996 Comparisons of experimental and numerical results for axisymmetric vortex breakdown in pipes. *Computers Fluids* **25**, 353–371.

DRAZIN, P. G. & HOWARD, L. N. 1966 Hydrodynamic stability of parallel flow of inviscid fluid. *Adv. Appl. Mech.* **9**, 1–90.

ESCUDIER, M. 1988 Vortex breakdown: observations and explanations. *Prog. Aerospace Sci.* **25**, 189–229.

ESCUDIER, M. P. & KELLER, J. J. 1983 Vortex breakdown: a two stage transition. *AGARD CP* 342, pp. 251–258.

FRAENKEL, L. E. 1956 On the flow of rotating fluid past bodies in a pipe. *Proc. R. Soc. Lond.* A **233**, 506–526.

GILBARG, D. & TRUDINGER, N. 1983 *Elliptic Partial Differential Equations of Second Order.* Springer.

HALL, M. G. 1967 A new approach to vortex breakdown. *Proc. Heat Transfer and Fluid Mechanics Institute, Univ. of California, San Diego, La Jolla*, pp. 319–340.

HALL, M. G. 1972 Vortex breakdown. *Ann. Rev. Fluid Mech.* **4**, 195–217.

HOWARD, L. N. & GUPTA, A. S. 1962 On the hydrodynamic and hydromagnetic stability of swirling flows. *J. Fluid Mech.* **14**, 463–476.

IOOS, G. & JOSEPH, D. 1980 *Elementary Stability and Bifurcation Theory.* Springer.

KELLER, J. J. 1995 On the interpretation of vortex breakdown. *Phys. Fluids* **7**, 1695–1702.

KELLER, J. J., EGLI, W. & EXLEY, W. 1985 Force- and loss-free transitions between flow states. *Z. Angew. Math. Phys.* **36**, 854–889.

KUFNER, A. 1983 *Weighted Sobolev Space.* John Wiley & Son.

LAMBOURNE, N. C. & BRYER, D. W. 1962 The bursting of leading-edge vortices-some observations and discussion of the phenomenon. *Aeronaut. Res. Counc. R & M* 3282, pp. 1–36.

LEIBOVICH, S. 1978 The structure of vortex breakdown. *Ann. Rev. Fluid Mech.* **10**, 221–246.

LEIBOVICH, S. 1984 Vortex stability and breakdown: survey and extension. *AIAA J.* **22**, 1192–1206.

LEIBOVICH, S. & KRIBUS, A. 1990 Large amplitude wavetrains and solitary waves in vortices. *J. Fluid Mech.* **216**, 459–504.

LEIBOVICH, S. & STEWARTSON, K. 1983 A sufficient condition for the instability of columnar vortices. *J. Fluid Mech.* **126**, 335–356.

LESSEN, H., SINGH, P. J. & PAILLET, F. 1974 The stability of a trailing line vortex. Part 1. Inviscid theory. *J. Fluid Mech.* **63**, 753–763.

LONG, R. R. 1953 Steady motion around a symmetrical obstacle moving along the axis of a rotating liquid. *J. Met.* **10**, 197–203.

LOPEZ, J. M. 1994 On the bifurcation structure of axisymmetric vortex breakdown in a constricted pipe. *Phys. Fluids* **6**, 3683–3693.

MALKIEL, E., COHEN, J., RUSAK, Z. & WANG, S. 1996 Axisymmetric vortex breakdown in a pipe-theoretical and experimental studies. *Proc. 36th Israel Annual Conf. on Aerospace Sciences* (*February*), pp. 24–34.

PECKHAM, D. H. & ATKINSON, S. A. 1957 Preliminary results of low speed wind tunnel tests on a gothic wing of aspect ratio 1.0. *Aeronaut. Res. Counc. C P* 508.

RANDALL, J. D. & LEIBOVICH, S. 1973 The critical state: a trapped wave model of vortex breakdown. *J. Fluid Mech.* **53**, 481–493.

RAYLEIGH, LORD 1916 On the dynamics of revolving fluids. *Proc. R. Soc. Lond.* A **93**, 148–154.

RUSAK, Z., WANG, S. & WHITING, C. H. 1996 Numerical computations of axisymmetric vortex breakdown in a pipe. *AIAA Paper* 96-0801.

RUSAK, Z., WHITING, C. H. & WANG, S. 1997 Axisymmetric breakdown of a Q-vortex in a pipe. *AIAA Paper* 97-0441.

SALAS, M. D. & KURUVILA, G. 1989 Vortex breakdown simulation: a circumspect study of the steady, laminar, axisymmetric model. *Computers Fluids* **17**, 247–262.

SARPKAYA, T. 1971 On stationary and traveling vortex breakdowns. *J. Fluid Mech.* **45**, 545–559.

SARPKAYA, T. 1995 Vortex breakdown and turbulence. *AIAA Paper* 95-0433.

SQUIRE, H. B. 1956 Rotating fluids. In *Surveys in Mechanics* (ed. G. K. Batchelor & R. M. Davies), pp. 139–161. Cambridge University Press.

SQUIRE, H. B. 1960 Analysis of the vortex breakdown phenomenon. *Miszallaneen der Angewandten Mechanik*, pp. 306–312. Berlin: Akademie.

STRUWE, M. 1990 *Variational Methods: Applications to Nonlinear Partial Differential Equations and Hamiltonian Systems.* Springer.

SZERI, A. & HOLMES, P. 1988 Nonlinear stability of axisymmetric swirling flows. *Phil. Trans. R. Soc. Lond.* A **326**, 327–354.

WANG, S. & RUSAK, Z. 1996*a* On the stability of an axisymmetric rotating flow. *Phys. Fluids* **8**, 1007–1016.

WANG, S. & RUSAK, Z. 1996b On the stability of non-columnar swirling flows. *Phys. Fluids* **8**, 1017–1023.

WANG, S. & RUSAK, Z. 1997 The effect of slight viscosity on near critical swirling flows. *Phys. Fluids* (submitted).

ZIEMER, W. P. 1989 *Weakly Differentiable Functions.* Springer.